Doctoral Dissertation

Academic Year 2017

Multi-Carrier Backscatter Communication System for Concurrent Wireless and Batteryless Sensing

Graduate School of Media and Governance
Keio University, Japan

Nitish Rajoria

Abstract

This research proposes a new multiple access method which enables concurrent wireless sensor data collection from multiple batteryless LSI sensors. This research is advantageous in the applications where long duration of synchronized sensor stream observation is demanded. The typical industrial application arena of the research is the integrity check of civil structures and machinery.

The batteryless wireless multiple access method is realized by employing the passive RFID mechanism to power up LSI sensors by the radio wave transmitted from a Reader/Writer. The radio reflection from an LSI sensor is either analog or digital modulated with an embedded sensor. To separate responses from multiple LSI sensors at the Reader/Writer, a non-orthogonal subcarrier is assigned to each LSI sensor. Although the non-orthogonal subcarriers can be produced only with a constant rate of antenna switching, they suffer from the mutual harmonics because of the physical nature of the signal shape. Because of these harmonics, the simultaneous usage of multiple subcarriers has not been much explored. Since the effectiveness of harmonic rejection method depends on the signal to interference ratio, optimal subcarrier allocation is essential. Therefore, the challenges of this research are two-fold. One is the harmonic rejection and the other is the optimal subcarrier allocation.

To cancel the harmonics, this research proposes a novel harmonic rejection method using digital signal processing with Hilbert and inverse-Hilbert transformation in the Reader/Writer. The method is implemented in a simulation and a prototype system with software defined radio platform LabVIEW and USRP. The method is evaluated with both simulation and physical experiment. It is revealed that the original signal can be recovered with 98 % cross-correlation accuracy even under 0 dB signal to interference ratio condition.

Since the subcarrier allocation is a combinatorial problem, obtaining the true optimal allocation requires vast amounts of examinations which are impracticable in a system where tens of LSI sensors are used. It is particularly evident when the variable distance and the variable

bandwidth required by LSI sensors. This research proposes a subcarrier allocation scheme based on a newly invented performance index, total contamination power, to prioritize indecision cases. The performance of the proposal is evaluated and compared with existing methods in terms of average communication capacity and system fairness using MATLAB Monte Carlo simulation. It is shown that the proposal can produce a subcarrier allocation which is equivalent to that of brute force method. While the brute force demands $O(n!)$ comparisons, where n represents the number of subcarriers, the proposal only demands $O(n^2)$ computations.

The practicality of the proposal is also evaluated in a vibration experiment where the proposal achieves equivalent performance compared with the wired sensors.

Keywords:

Backscatter Communication, Multiple Access, Sensor RF tag, Harmonic Rejection, Subcarrier Allocation

Acknowledgement

First and foremost, I would like to express my sincere gratitude to my advisor Dr. Jin Mitsugi for his valuable guidance, constant encouragement, and discussion during the course of this research. He was extremely patient to discuss the research details with me and providing valuable feedback. I have learnt various technical concepts and skills from him which will help me throughout my career. I really enjoyed working with him and feel fortunate to be part of his research group since he is very concerned for his students.

I am also grateful to my co-advisors Dr. Jun Murai and Dr. Osamu Nakamura for giving valuable suggestions during the presentation. I would like to thank Dr. Rod Van Meter for his valuable suggestions and especially for the proofreading of my research papers. I always enjoyed the friendly discussions and social time with them after the d-camp presentation. I also thank Dr. Kotaro Kataoka who introduced me to Dr. Jin Mitsugi, a great person, and professor.

I am very thankful to my laboratory colleagues and people of Japan for providing a welcoming environment. I am thankful to Yuki Sato, Yuki Igarashi, Hiromu Kamei, Iori Mizutani, Lisa Obata, Kohei Yamamoto for their social companionship and hospitality which has helped me through this journey. I may have missed some individuals I interacted with, but would like to thank them who have directly or indirectly helped me towards carrying out this research.

I would like to make a special mention of the excellent facility provided by Auto-ID lab, Keio University, Japan. Such a conductive research environment is a significant part in accomplishing this work. I also express my thanks to Japan International Cooperation Agency (JICA) for the support and research opportunity offered to me.

Finally, I am thankful to my family for supporting and motivating me throughout all of my studies.

Contents

List of Figures

List of Tables

Chapter 1

Introduction

1.1 Background

Many civil structures such as bridges and buildings are constructed during the period of high economic growth. In Japan's case, it was 1960s and 1970s. This infrastructure will be inevitably aging in the next twenty years. Civil structures 50 years old after construction are considered to be end-of-life yet are expected to increase quickly [1] as shown in Fig 1.1. Depending on the relevant laws and inspection procedures, it is mandatory to conduct regular visual inspection and detailed diagnostic inspection [2]. For road structures, the Road Law Enforcement Regulations Inspection is mandatory. For example, bridge beams need to be inspected every 5 years according to the unified standard set by the country. Such inspections entail both the financial cost and human labor. A lack of such inspection sometimes results in tragic accidents such as the collapse of Sasago tunnel ceiling in Japan in December 2012 and Kolkata flyover collapse in India in March 2016. The Sasago accident was attributed to the imperfect implementation of anchor bolts according to the report compiled by Japanese government [3]. Such accidents have led to research focused on health monitoring of large civil structures. For that Structural Health Monitoring (SHM) now even planned during the design phase of the structure. If SHM can be realized with wireless and batteryless implanted sensors,

the target structures can be examined more often and in detail with lower cost, which surely will mitigate safety risk. Similar demands toward the batteryless and wireless measurement can also be found in relatively small yet complex and delicate structures, such as rotating machines and space structures. This is why batteryless wireless SHM attracts significant technical interests [4, 5, 6, 7, 8].

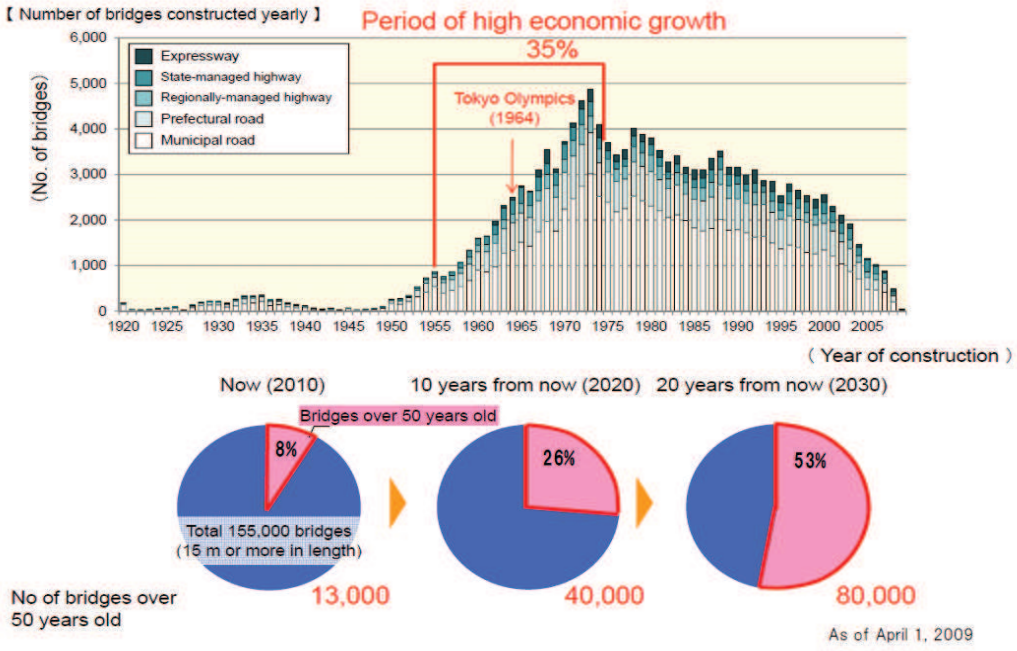

Figure 1.1: Civil structures are rapidly aging in Japan [9]

Vibration testing is a commonly used method in SHM. Figure 1.2 shows a vibration testing of an artificial satellite. There are a number of vibration sensors attached to the body of the satellite and each sensor is connected to the power source and the signal processor. Wire harnesses shall be carefully routed not to damage the mechanical characteristics and also the delicate structure. This is the typical setting of vibrational testing to measure frequency response of a structure. Concurrent data collection needs to be done from multiple sensors mounted at different location to establish the frequency response of the structure against an exciting force.

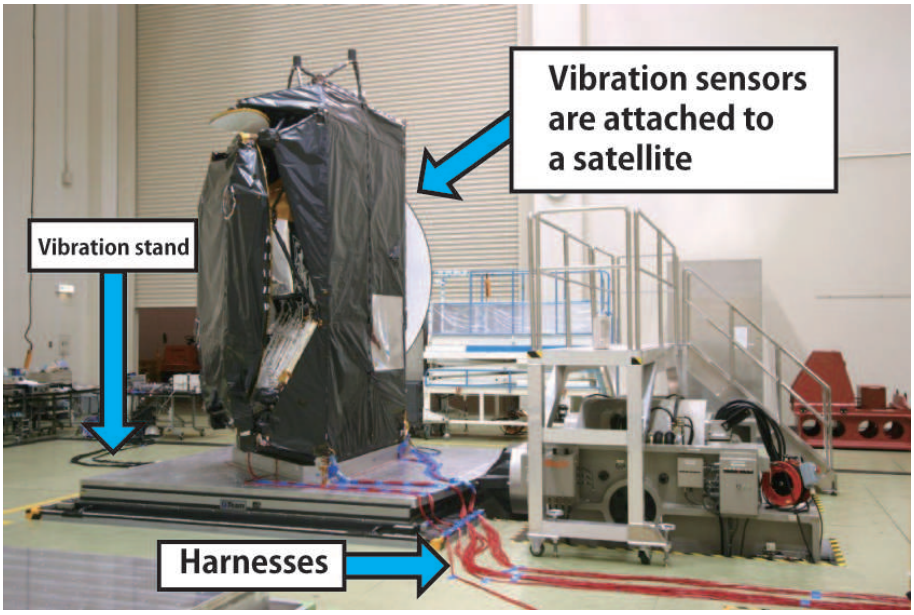

Figure 1.2: An artificial satellite subjected to vibrational testing (source: Japan Aerospace Exploration Agency)

1.2 Challenges in Wireless Sensor Network (WSN) for Structural Health Monitoring (SHM)

The application of WSN for SHM has a number of challenges and requirements. Noel [10] provides a good review on the requirement and survey in this field. There is a comparison between wired and wireless sensor networks as shown in Table 1.1.

In the comparison, it is shown that WSN are advantageous for their easy deployment, cost and time. The weak points are the lifespan (because of the battery), bandwidth, data rate and the synchronicity. The dominant frequency for strain measurement is lower than 1Hz and up to several kHz in vibration testing [11, 12]. Considering the available bandwidth for WSN in world radio regulations is around several hundred kHz, it should not be a critical problem particularly for less than 100Hz frequency domain system. The inherent weak point of wireless sensors is the battery replacement even though there is a number of technologies advocating low power. If we can realize batteryless and wireless sensors, not would be a big

Table 1.1: Comparison of wired and wireless sensor networks, cited from [10]

Metric	Wired Sensor Network	Wireless Sensor Network
Cost	Very high	Low
Deployment time	Very long	Short
Lifespan	Long	Short typically limited by node battery lifespan
Number of sensors	Typically low	Typically higher due to ease of sensor installation
Connection bandwidth	High	Limited
Data rate	High	Lower
Sensor synchronicity	Very high	Concern due to wireless connection

impact. A another big challenge of WSN for SHM is the synchronization of sensor nodes. To detect and localize a damage, a tight time synchronization, below 120 μs [13] is required. The synchronicity is required to accurately measure the vibration phases. Unless the accuracy is achieved, the vibration testing may fail. On the other hand, the permissible measurement delay is not stringent. As it discusses later in this dissertation, the synchronicity of wireless sensors is usually achieved by employing Frequency Division Multiple Access (FDMA) or Code Division Multiple Access (CDMA). But FDMA demands wireless sensors to furnish variable carrier frequency oscillator and a channel filter. This contradicts the requirement of low power. On the other hand, CDMA only demands high clock rate to produce a spreading code but the degree of concurrency is inherently low because of the near/far problem. The requirement on the number of sensors in SHM is studied in [11] to be up to 70.

1.3 Research Objectives

The purpose of this research is to provide a new multiple access method tailored to SHM using wireless and batteryless sensors. This research has the following main requirements:

- The time synchronization should be below 120 μs.
- The number of channels is up to 70 and at least 50.

- The target frequency bandwidth for one channel is up to 100Hz.
- The proposed system should be implemented and verified with a vibration testing.

1.4 Contributions

The main contributions of this research are followings.

- The theory of new multiple access, Multiple Subcarrier Multiple Access (MSMA), is established and verified with simulations and experiment.
- A channel allocation scheme is invented, referred to as total contamination power, which can be applied to variable distance and variable bandwidth MSMA system.
- A software based receiver prototype is developed with LabVIEW and USRP.

1.5 Dissertation Organization

This dissertation has six chapters as graphically represented in Fig.1.3. The chapters are organized as follows:

Chapter 1 explains the background of this research and its objectives.

Chapter 2 explains the backscatter communication system and overview of proposed multiple access method referred to as MSMA. This chapter briefly explains the two primary challenges, harmonic rejection and channel allocation, in MSMA. It also discusses existing multiple access techniques such as Time Division Multiple Access (TDMA), FDMA and CDMA and their limitations. This chapter further discusses the related works in this area.

Chapter 3 explains the mathematical model of harmonic rejection method in MSMA. This chapter explains the difficulties to calculate the phase delay and group delay of carrier wave and subcarrier, respectively. This chapter shows a PLL method can be used to calculate the

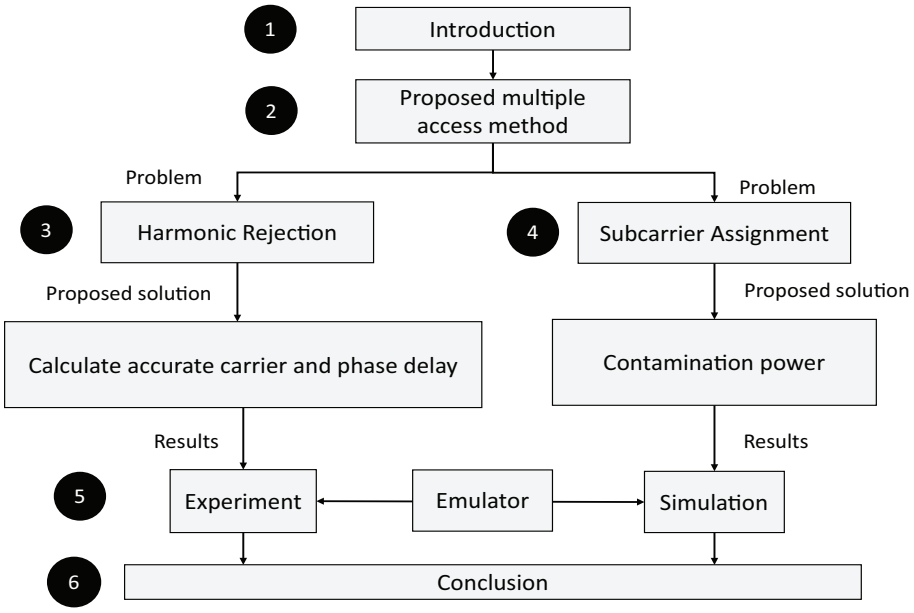

Figure 1.3: Structure of the dissertation

carrier delay. It also explains the method to calculate accurately the replica of harmonic using Hilbert transformation and inverse Hilbert transformation. Further it explains the performance of harmonic rejection method depending on the Carrier to Interference Ratio (CIR) of a subcarrier.

Chapter 4 formulates the subcarrier allocation problem to improve the total communication capacity. Further, the subcarrier allocation problem is divided into two subproblems which are fixed bandwidth subcarrier allocation and variable bandwidth subcarrier allocation. This chapter examines different subcarrier allocation schemes and reveals that allocating near (near to central frequency) subcarrier to far wireless sensor gives better results. However, in the variable bandwidth subcarrier, this scheme does not perform well. This chapter proposes a new allocation scheme based on the total contamination power. In the end, this chapter finds that the subcarrier allocation based on the total contamination power performs better for both fixed bandwidth and variable bandwidth subcarrier allocation.

Chapter 5 explains the setup and results of a vibration testing to show the performance of

the proposal. This chapter also compares the results with a commercial wired vibration testing system and MSMA.

Chapter 6 presents the conclusion of this research.

Chapter 2

Overview of MSMA and Related Works

2.1 The Idea of Multiple Subcarrier Multiple Access (MSMA)

In the process of seeking a good way to realize batteryless, wireless and concurrent sensor data collection, an idea of using passive RFID technology emerged. The principle is based on the backscatter wireless communication mechanism which is extensively used in passive RFID and radars [14]. The best feature of MSMA is to allow concurrent sensor data streaming from multiple batteryless sensors. The use of backscatter wireless communication to transfer not only unique ID of physical objects but also sensor data is an emerging research field [15, 16].

To introduce MSMA, first, the backscatter communications principle is explained. The concept of MSMA and its challenges are introduced in the following subsections.

2.1.1 Backscatter Wireless Communications Principle

Typical backscatter wireless communications system is passive RFID in the UHF (860-960MHz) band. The system is extensively used in supply chain management (SCM) applications where tiny, low cost RF tags are attached to physical objects. The location and disposition of the physical objects are shared among stakeholders via a standardized information platform [14, 17].

The non-line-of-sight long range communication, fast inventory of RF tags and writing function distinguish UHF RFID from other automatic identification technology such as bar-code and NFC.

A passive RFID system comprises a Reader/Writer and multiple RF tags. The RF tag is powered by the continuous wave (CW) provided by the Reader/Writer and processes the commands. The tag-to-reader link is established by changing the antenna impedance of the RF tag with an embedded RF switch, as shown in Fig.2.1. Multiple access from RF tags to Reader/Writer is usually based on TDMA, specifically frame slotted ALOHA. An RF tag under inventory requests a time slot with a random number. If the request is granted, Reader/Writer transmits an acknowledge with the random number. If the RF tag receives a proper acknowledgment, it backscatters its unique ID. If there is a collision of multiple RF tags in one time slot, Reader/Writer does not acknowledge and the RF tags postpone the transmission to the next communication frame.

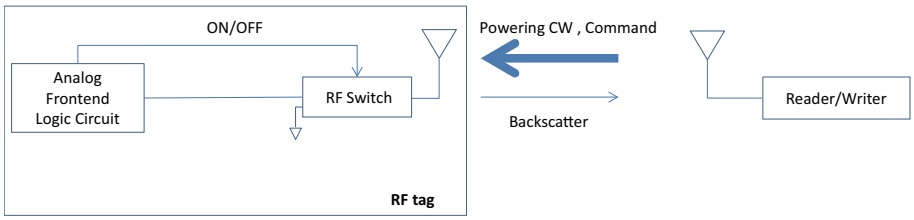

Figure 2.1: Passive RFID enables a batteryless RF tag to send signal by changing the antenna impedance.

When sensor data needs to be collected, a sensor connected RF tag which is referred to as "sensor RF tag" in this dissertation is used. Since the existing multiple access method in the sensor data collection is also TDMA, it is difficult to send sensor streams concurrently from multiple sensor RF tags.

The communication distance between an RF tag and Reader/Writer is, in many cases, dominated by the reader-to-tag link, which powers RF tags. When there is a high sensitivity RF tag, the second bottleneck of reading distance is the phase noise of the Reader/Writer. Since the phase noise diminishes as wide frequency separation is taken from the powering CW,

many UHF RFID system employ subcarrier backscatters by superposing a constant rate on/off keying to the digital data. The spectrum of normal backscatter and subcarrier backscatter are illustrated in Fig.2.2.

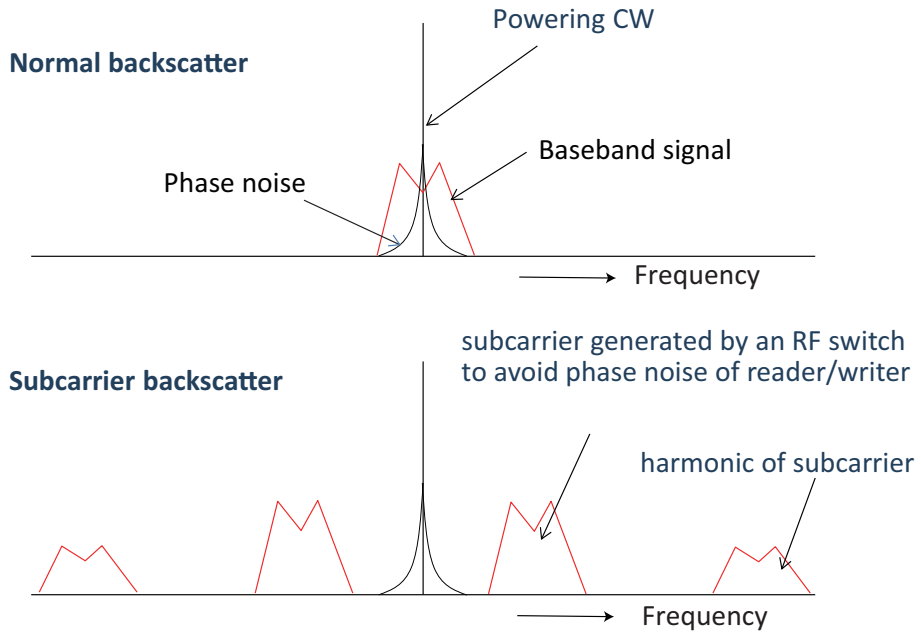

Figure 2.2: By adding constant rate on/off keying to the data, backscatter signal can separate from the phase noise of powering continuous wave.

The subcarrier backscatter is advantageous to avoid phase noise with the penalty of less bandwidth. Also, the inherently weak backscatters can be protected from neighbor Reader/Writers. Since a subcarrier is produced by a constant rate on/off keying without any channel filter, the subcarrier backscatter entails harmonics. Because of these harmonics, the simultaneous usage of multiple subcarriers has not been considered nor tried so far.

2.1.2 MSMA Overview

MSMA is a pseudo-frequency division multiple access (FDMA) using multiple subcarriers simultaneously, as shown in Fig.2.3.

The high-level protocol of MSMA is shown in Fig.2.4. The Reader/Writer first inventories

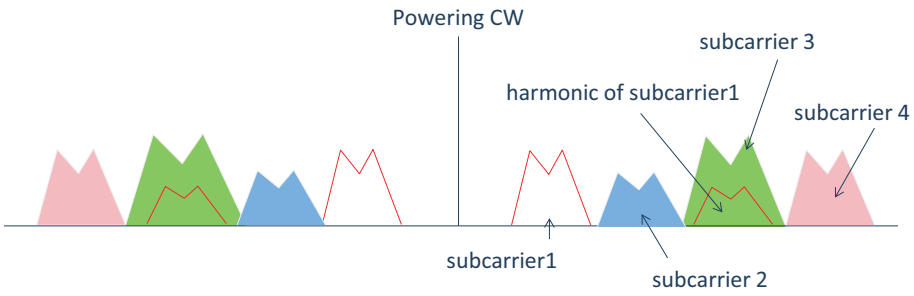

Figure 2.3: MSMA uses multiple subcarriers enabling concurrent sensor data stream collection.

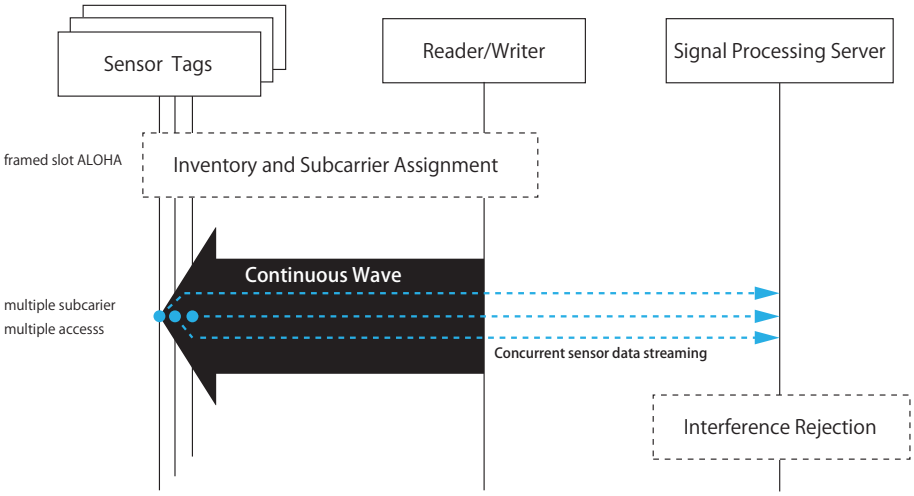

Figure 2.4: Multiple subcarrier multiple access has two phases. In the first phase, the Reader/Writer inventories sensor tags with conventional frame slotted ALOHA. In the second phase, the Reader/Writer transmits continuous wave which powers sensor tags to allow concurrent data streaming's.

RF tags with conventional frame slotted ALOHA. This way, the Reader/Writer collects all the unique IDs of RF tags in the interrogation field with their RSSIs. After the inventory, the Reader/Writer allocates a dedicated subcarrier frequency to each sensor RF tag based on the RSSI and required bandwidth. Next, the Reader/Writer transits into the "listen" state where the Reader/Writer receives the sensor data stream. Therefore, it is obvious that MSMA is advantageous in the applications where long duration of synchronized sensor stream observation is demanded such as vibration testing of machinery and continuous surveillance and monitoring.

The superposing of the sensor stream onto the backscatter signal can be done either by digital or analog modulation. In digital modulation, sensor data is firstly sampled and quantized with an analog-digital converter (AD converter). The digital sensor data is superposed on the subcarrier by taking the exclusive OR of sensor data and subcarrier bits. In analog modulation, the AD converter can be eliminated in the sensor RF tag.

If a harmonics rejection method is developed which allows concurrent analog streams, the method can apply to digitally modulated signal agnostic to the modulation and coding scheme. This strategy, in return, demands a sophisticated rejection method. A sensor RF tag in MSMA can thus be produced just by adding a sensor and a modulator to the RF tag, as shown in Fig.2.5.

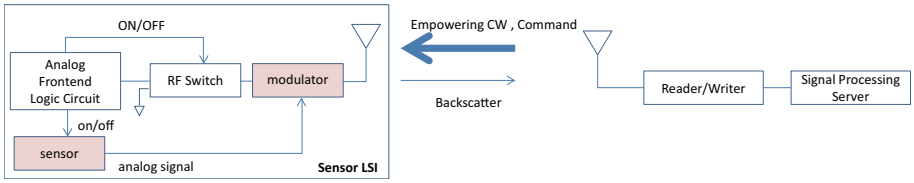

Figure 2.5: A typical schematic of sensor RF tag in MSMA

2.1.3 MSMA Challenges

There are two challenges in MSMA as follows.

1. Harmonics Rejection Method: In MSMA, the unavoidable mutual interference among subcarriers, because of the harmonics, takes place and should be rejected. The main problem is to accurately produce replicas of primal subcarrier harmonics. This is further explained in the Chapter 3.

2. Subcarrier Allocation: As the sensor RF tag's locations are chosen to tailor the application demand, Carrier to Interference and Noise Ratio (CINR) of a tag-to-reader link depends on the sensor RF tag's location and propagation characteristics. Since the subcarrier which is close to the powering CW produces more harmonics into the rest of the

channels than that of the subcarrier which is far from the CW, it is required to allocate subcarriers to the sensor RF tags in an efficient way to improve the overall communication capacity of the system. This is further explained in the Chapter 4.

2.1.4 Multiple Access Methods

Multiple access is a method which arbitrates the accesses from multiple wireless sensors. The commonly used multiple access methods are:

- Time Division Multiple Access (TDMA)
- Frequency Division Multiple Access (FDMA)
- Code Division Multiple Access (CDMA)

Time Division Multiple Access (TDMA)

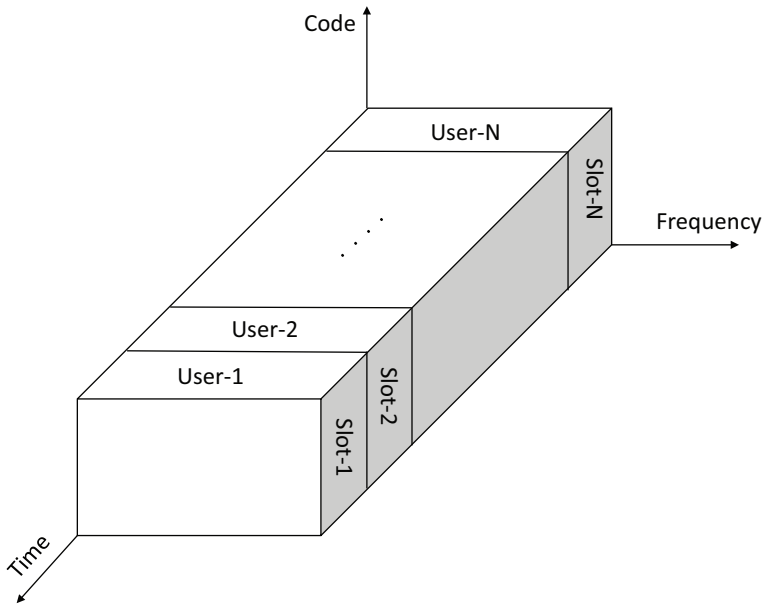

Figure 2.6: Time Division Multiple Access

TDMA is digital transmission method that allows a number of wireless sensors to access a frequency band without causing interference by allocating dedicated time slots to every wireless sensor as shown in Fig.2.6. A wireless sensor can access the frequency band only in its time slot for transmitting its data. The wireless sensor and the receiver should have the same clock for the time synchronization so that the time slots do not overlap. Applying TDMA in a sensor RF tag requires time synchronization and large buffer to store the data while waiting for the allowed time slot to transmit the data, therefore it is prohibitive.

Frequency Division Multiple Access (FDMA)

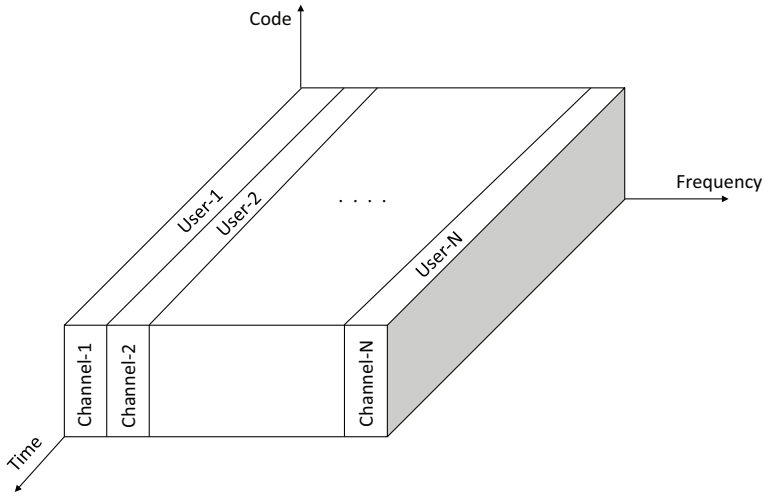

Figure 2.7: Frequency Division Multiple Access

In FDMA, the frequency band is divided into the multiple channels as shown in Fig.2.7. The method carries out communication by allocating channels to each wireless sensor. All wireless sensors can access the frequency band at the same time by using their allocated channels. A wireless sensor is required to have a channel filter to reduced the adjacent channel interference. Applying FDMA in a sensor RF tag is prohibitive because of the absence of local oscillator and the adaptive channel filter to produce various channel frequency.

Code Division Multiple Access (CDMA)

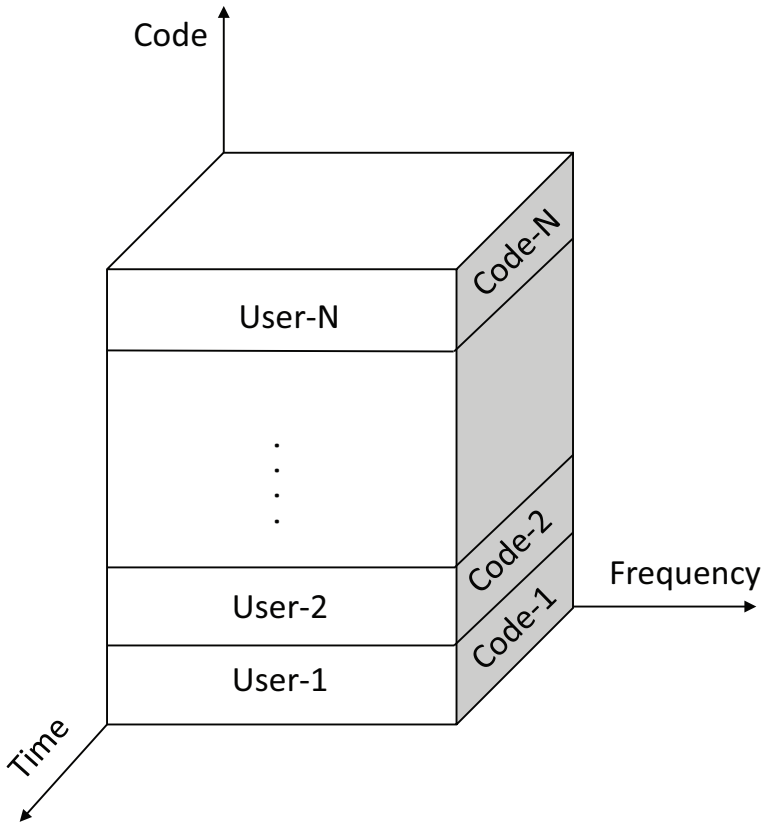

Figure 2.8: Code Division Multiple Access

In CDMA, instead of dividing frequency band into channels or time slots, each wireless sensor uses a unique code which spreads the signal into the whole frequency band. Wireless sensors can transmit the spreaded signal simultaneously. The receiver can recover the original signal by de-spreading the mixed signal. The transmission power control to adjust CIR at the receiver is difficult in the passive communication system. Applying CDMA in a passive communication system significantly decreases the available number of channels because it cannot realize the transmission power control. In [18], the dynamic framed slotted ALOHA technique is replaced with the CDMA technique to improve the tag identification procedure. However, the results are shown with the MATLAB numerical simulation and the location of

wireless sensors are not defined.

2.2 Related Works

Many schemes have been proposed for sensing the acceleration, strain, displacement and vibration in structural monitoring. Among these, RFID-based methods [19, 20] have become increasingly popular. Especially, passive RFID is an emerging technique where a passive tag transfers the sensor data, which includes, for example, temperature, humidity and density of chemical compounds as well as acceleration and strain and relative displacement. A contactless loading sensor system that can measure the internal loading of an object structure through several covering materials for the purpose of SHM is developed in [21]. The authors proposed an architecture by which two RFID tags are used in the passive system. The functions of the tags are separated for communication and for the power supply as a circuit design contraption to solve the power supply problem. However, authors do not introduce the multiple sensors environment. An RFID based sensor design is introduced in [22] for completely passive UHF RFID sensor for strain monitoring starting from a flexible meander-line dipole whose shape factor and feed section are engineered to achieve the desired sensing resolution and dynamic range for structural health monitoring of damaged structures.

Following sections provide a review of the related works in the two challenges of MSMA mentioned previously: harmonic rejection and subcarrier allocation.

2.2.1 Related Works on Harmonic Rejection

An analog data transmission over a backscattered subcarrier can be found in a classic literature [23], the paper also explains the basic theory for reflected power communication with reference to conventional radar transmission, and the law of propagation is derived and compared with the propagation law for radar.

In [24], the properties of analog backscatter and digital backscatter are compared. The

authors proposed a combination of the two that can provide a solution for high data rate battery free wireless sensing. Authors also present a hybrid analog-digital backscatter platform that uses digital backscatter for addressability and control but switches into analog backscatter mode for high data rate transmission of sensor data. However, multiple subcarrier transmission is not discussed.

Multiple subcarriers transmission is common place in OFDM or optical communications [25]. However with a presumption that the terminals are intelligent enough to perform digital signal processing such as the inverse FFT.

In [26, 27], the application of backscatter communication for data uplink from sensor nodes interrogated by an Frequency Modulated Continuous Wave (FMCW) radar in addition to its primary use in area surveillance is introduced. This paper also shows the feasibility of proposed system, but it seems to be difficult to avoid inter-modulation if some sensors are located in the same distance.

In [28], a practical design of an RFID Reader/Writer that is capable of reading multiple passive tags through joint decoding is presented. Figure 2.9 shows the block diagram of modi-

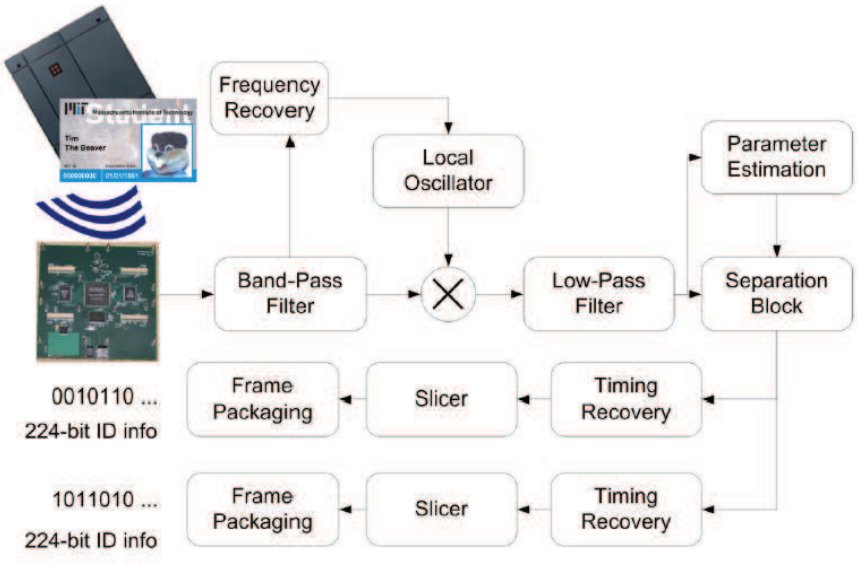

Figure 2.9: System block diagram with modifications for decoding multiple RFID cards [28]

fication for decoding multiple RFID cards. The work is similar to this research whereas it does not receive interference from other subcarriers. They uses the advanced signal processing techniques to achieve multiple source signal separation rather than higher layer MAC scheduling. The authors derive the channel model from measurements and observations made from the Indala LF 125kHz Proximity RFID card system. The basic idea of the signal separation is decoding each received symbol by seeking the closest constellation point with the shortest Euclidean distance, then mapping the point back to a length-N bit sequence, thus achieving separation of multiple card signals. The main limitation of this approach is that it does not support the continuous streaming signal. Also this work at the receiver may not be practical for hardware implementation because the study assumes that signals are digitally modulated and their IQ constellations are calibrated first and can be discriminated with each other with the calibration.

In [29] a concurrency-based protocol based on the idea using compressive sensing decoding is introduced. Initially all the nodes transmit in a synchronous bit-by-bit manner, so the received signal can be expressed as:

$$y = A \begin{bmatrix} h_1 x_1 \\ . \\ . \\ h_N x_N \end{bmatrix} = A \begin{bmatrix} h_1 & & & \\ & . & & \\ & & . & \\ & & & h_N \end{bmatrix} x = AH_X = Az \tag{2.1}$$

where y, the received symbol at the reader, is a linear combination of the complex channel coefficient corresponding to node i. $H_{N\times N}$ is a diagonal channel matrix and $H_{i,i} = h_i$ is the complex channel coefficient of the i^{th} node. x is sparse randomized matrix $i.e$ it has only non zero entries. Once the randomization matrix and the channel coefficients from each node are known, the function can be inverted to estimate the bits transmitted by each tag. However, to implement this method in practice is very challenging. One practical problem is the clock of all nodes need to be synchronized. Another problem is channel coefficient need to be reestimate

according to the node position.

The another approach for separation of signal is presented in [30]. The phase and amplitude information (IQ vector) creates multiple cluster when the tags transmit simultaneously. The each cluster corresponds to a specific combination of values from the tags. This approach could be viewed as the unstructured analogue of methods like Quadrature Amplitude Modulation (QAM). While the signals in QAM are structured to be as far apart as possible, the clusters in this case are unstructured and depend on channel coefficients between each node and the reader. The main limitation of this approach is simply it does not work perfectly when the number of nodes are increased.

In [31], authors use the time envelop to extract collided signal information to enable concurrent sensor data streaming. Since all the existing studies are subjected to ASK, they require another IQ data calibration every time the sensor RF tags or the Reader/Writer change their position and orientation, besides the moving tags and moving Reader/Writers. The sampled and quantized sensor signal needs to be digitally superposed onto the subcarrier signal, which inevitably expands the frequency bandwidth. Even when the minimum sampling rate (double the Nyquist frequency) is assumed and 8 bits quantization. The required bandwidth expands by a factor of sixteen times compared to analog streaming.

The rejection of analog harmonics caused by the nonlinearity of amplifiers has been studied since the 1960s. Recently the use of digital signal processing for the harmonics process is studied. In [32], a dual-frequency radar, which estimates the range of a target based on the phase difference between two closely spaced frequencies, has been shown to be a cost-effective approach to accomplish both range-to-motion estimation and tracking. The proposed approach suffers from two drawbacks: it cannot deal with multiple moving targets, and it has poor performance in noisy environments. The authors proposed the use of time-frequency signal representations to overcome these drawbacks.

Another problem associated with a wideband receiver is that when the local oscillator (LO) tunes a channel at the lower end of the receiver passband, say, around 900 MHz, the square

wave commutation mixes unwanted channels at the third and fifth harmonic of the LO which also lie in the passband. These channels also appear at zero-Intermediate Frequency (zero-IF). This effect can only be suppressed by somehow "linearizing" the mixing action. A hard switching mixer is always preferred because it gives the best conversion gain. The harmonic content associated with hard switching can be lowered by shaping the commutation square wave into a step-wise waveform resembling a sine wave; more precisely, a waveform that corresponds to samples of a sine wave. Theoretically, this commutation waveform has no third or fifth harmonic [33]. Figure 2.10 shows the block diagram of two step of harmonic rejection transmitter. The unique mixers used in the baseband to IF upconversion. This transmitter maintains the performance advantages of the traditional indirect upconversion transmitter in that both LO pulling and LO feedthrough are reduced.

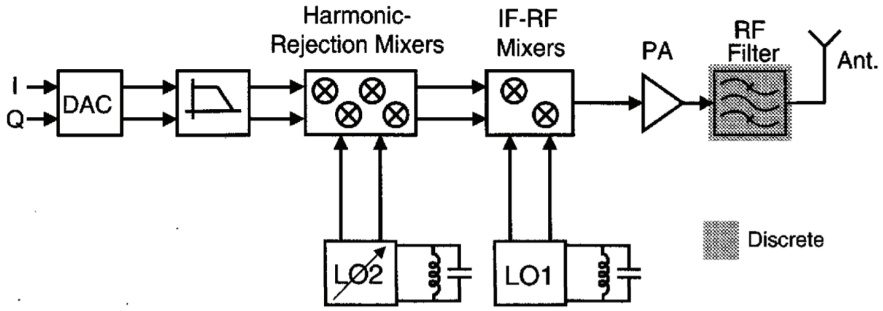

Figure 2.10: Harmonic-rejection transmitter block diagram [33]

In [34] an alternative digital intensive architecture, which enables increased harmonic interference rejection for wide-band SDR transceivers impacted by severe gain and phase mismatches. Figure 2.11 shows the multi-path recombination (weighting and summing) stage to the digital domain which is abbreviated as DRDC (digital recombination and digital compensation). After low pass filter (LPF), the multi-path recombination process is performed in the digital domain. Although the fundamental idea of rejecting harmonics is applicable to the backscatter signals, these existing studies do not consider the phase delay, which demands delicate handling of backscatter signals.

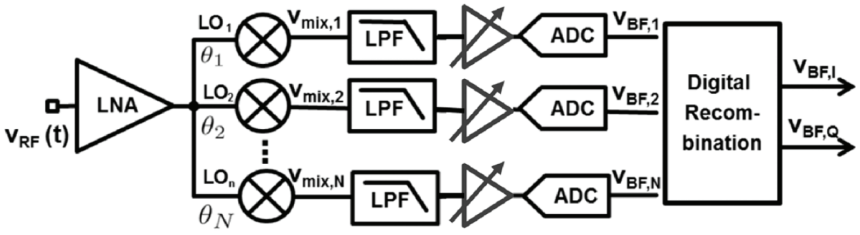

Figure 2.11: Generic block diagram for digital multi-path harmonic rejection. [34]

In [35] a short code is used instead of long code to spread the signal over the band which is similar to MSMA. Orthogonal frequency code (OFC) is used for spread-spectrum that employs frequency and time diversity. OFC is a coding technique used to spread the signal bandwidth between several frequencies that are defined to be orthogonal to each other. As the reflector length increases, the reflected power increases and the bandwidth of the frequency response decreases as shown in Fig.2.12. The main limitation of this approach is to rely on the spreading code. Also, they do not consider the harmonics effect.

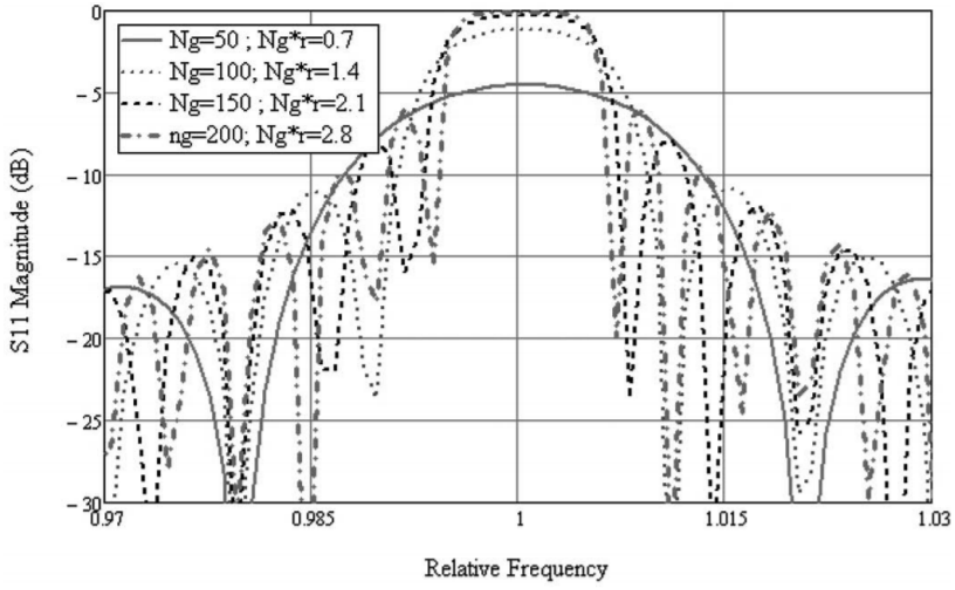

Figure 2.12: Frequency responses of a reflector chip with varying reflector lengths. [35]

In a passive optical system, subcarrier multiple access (SCMA) was presented in the 1990's

[36]. In SCMA, a distinct subcarrier frequency is assigned to each subscriber. Signals produced by subscribers are transferred as the subcarrier of light source.

Although the generation and usage of the subcarrier is similar, MSMA can be applied to a system which only has an RF switch. Also the original signal is effectively recovered by applying signal processing at the Reader/Writer side.

2.2.2 Related Works on Subcarrier Allocation

Subcarrier allocation problem is also investigated in OFDMA field. In [37], [38], several subcarrier allocation schemes based on a game theory are proposed for achieving channel gain and power allocation. Such allocation schemes are not applicable in sensor RF tags, because even basic signal processing such as inverse FFT and channel filtering are prohibitive in batteryless backscatter communication system.

In [39], four classes have been defined based on the required sensor application data rates. An utility function is associated with each class where utility is a function of achievable data rate. The main aim of this approach is to maximize the aggregate throughput by maximizing the aggregate utility. But, in this approach, priority and fairness of sensors are ignored.

Dynamic programming such as knapsack problem could be applied to the channel allocation problem. But the existence of infinite harmonics in the multiple subcarrier system complicates the problem particularly when the variable subcarrier bandwidth is allowed.

2.3 Summary

This chapter reviews the passive RFID system based on the backscatter communication system. Various multiple access techniques and their limitations with regard to multiple sensor RF tag application are discussed. Related works in the field of MSMA, harmonic rejection and subcarrier allocation are also discussed.

Chapter 3

MSMA: Harmonic Rejection Method

3.1 MSMA Subcarrier Communication System

This section provides the overview of the conventional subcarrier passive communication system and then introduces the multiple subcarrier multiple access communication system.

3.1.1 Conventional Subcarrier Communication System

A passive communication system comprises a Reader/Writer and sensor RF tags enabling bi-directional communication links without implementing a power source, such as a battery, in the sensor RF tags. The communication link from a sensor RF tag and a Reader/Writer is enabled by modulated backscatter which is produced by changing the antenna impedance of the sensor RF tag, most commonly with an RF switch. Since a sensor RF tag is powered by the radio wave from the Reader/Writer, the Reader/Writer supplies a continuous wave even while the sensor RF tags are responding. The major noise received by the Reader/Writer is usually the phase noise of continuous wave (after reflection by sensor RF tag). A common practice to avoid the phase noise is to separate the signal of sensor RF tags from the continuous wave. This can be realized by changing the antenna impedance at a constant rate, which referred

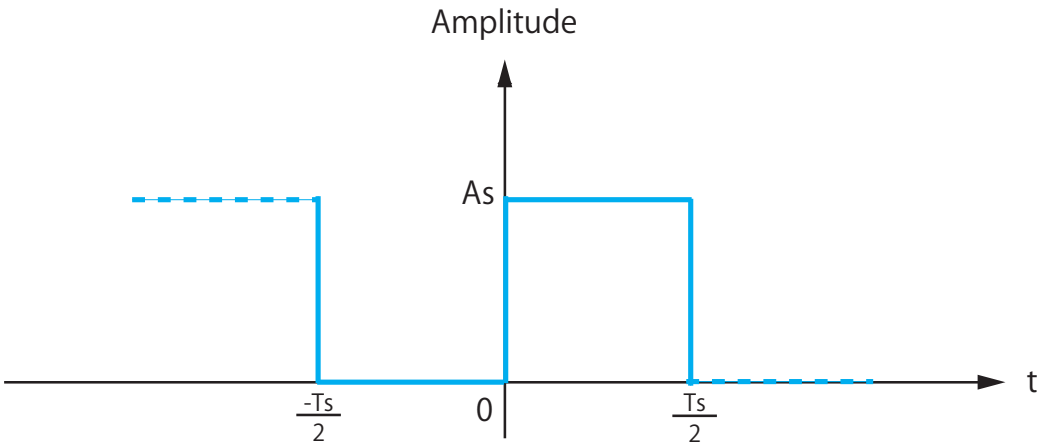

Figure 3.1: The infinite square wave in time domain representing subcarrier signal whose frequency is $\frac{1}{T_s}$

as the subcarrier frequency in this dissertation. The reflected signal from a sensor RF tag, therefore, is a modulated subcarrier. The baseband signal can be either digital or analog. If the subcarrier frequency denoted as f_s and the subcarrier period as $T_s = \frac{1}{f_s}$, the time domain subcarrier signal can be represented by an infinite repetition of the elemental signal as shown in Fig. 3.1.

The subcarrier signal in time domain $s_e(t)$ can be expressed by the following equations, where A_s is the amplitude of square waveform signal.

$$s_e(t) = \begin{cases} 0 & (-\frac{T_s}{2} \leq t \leq 0) \\ A_s & (0 \leq t \leq \frac{T_s}{2}) \end{cases} \tag{3.1}$$

The frequency response of the square wave can be derived by applying Fourier expansion Eq.3.2. In Eq. 3.2, L represents true interval.

$$f(t) = \frac{a_0}{2} + \sum_{n=1}^{\infty}(a_n \cos\frac{n\pi t}{L} + b_n \sin\frac{n\pi t}{L}) \tag{3.2}$$

In the case of Fig. 3.1, L in Eq. 3.2 is set to $\frac{T_s}{2}$. In Eq.3.2, a_0 can be derived from below

Eq.3.3.

$$\begin{aligned} a_0 &= 2f_s \int_0^{\frac{T_s}{2}} 1 \; dt \\ &= 1 \end{aligned} \tag{3.3}$$

a_n can be derived from the Eq. 3.4.

$$\begin{aligned} a_n &= 2f_s \int_0^{\frac{T_s}{2}} \cos 2\pi n f_s t \; dt \\ &= 0 \end{aligned} \tag{3.4}$$

b_n can be derived from Eq. 3.5 below.

$$\begin{aligned} b_n &= 2f_s \int_0^{\frac{T_S}{2}} \sin 2\pi n f_s t \; dt \\ &= \frac{1 - \cos n\pi}{n\pi} \end{aligned} \tag{3.5}$$

Finally, the frequency response of the square wave $s_e(t)$ is shown in Eq.3.6.

$$s_e\left(t\right) = A\left\{\frac{1}{2} + \sum_{n=1}^{\infty} \frac{1 - \cos n\pi}{n\pi} \cdot \sin 2\pi n f_s t\right\} \tag{3.6}$$

The summation part of this equation can be rewritten as the following.

$$\frac{2}{\pi}\left(\sin 2\pi f_s t + \frac{1}{3}\sin 2\pi\left(3f_s\right)t + \frac{1}{5}\sin 2\pi\left(5f_s\right)t + \frac{1}{7}\sin 2\pi\left(\,7f_s\right)t \ldots\right) \tag{3.7}$$

This shows that a square waveform envelope whose fundamental frequency is f_s contains harmonics components and phase at the odd number n multiples ($3f_s$, $5f_s$, $7f_s$, ...) and the amplitude of each frequency component is $\frac{1}{n}$ ($\frac{1}{3}$, $\frac{1}{5}$, $\frac{1}{7}$, ...). This theoretical harmonics and their amplitude ratio are examined in an experiment. Figure 3.2 shows the comparison between

measured power spectrum and theoretical one at the frequency $f_c + f_s n$ (n =3, 5, 7, 9, 11, 13, 15, 17, 19, 21, $n = 1$ as the cardinal point), where the carrier frequency f_c is 916.80MHz and the fundamental subcarrier frequency f_s are 30kHz so that primal subcarrier frequency is set to 916.83MHz. The measured spectrum almost agrees with the theoretical one, so this

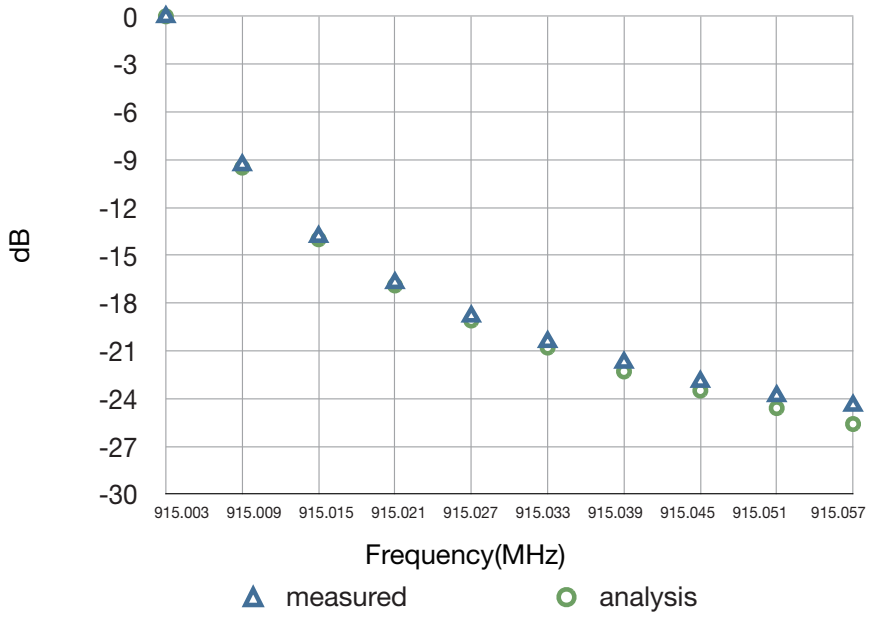

Figure 3.2: Experimental verification of the decay of subcarrier harmonics

result proves the validity of the above-mentioned amplitude ratio between the subcarrier and its higher harmonics components. However, there are still slight difference between theoretical one and measured one. The attenuation of the subcarrier signal is also depends on modulation index which is difficult to derive mathematically because it relates to the impedance matching of sensor node's antenna. This amplitude ratio information enables the interference rejection from the simultaneously transmitted multiple subcarrier signals.

It is shown that harmonic components emerge at the odd multiples of primal subcarrier frequencies. The power of the harmonics decays rapidly. The subcarrier signal is applied to a

carrier frequency f_c in an amplitude modulation manner to produce the subcarrier RF signal.

$$\begin{aligned} S(t) &= s_e(t)e^{j2\pi f_c t} \\ &= \frac{A_s}{2}e^{j2\pi f_c t} + \frac{A_s}{j\pi}\left\{e^{j2\pi(f_s+f_c)t} - e^{-j2\pi(f_s+f_c)t}\right\} \\ &+ \frac{A_s}{3j\pi}\left\{e^{j2\pi(3f_s+f_c)t} - e^{-j2\pi(3f_s+f_c)t}\right\} + \\ &+ \frac{A_s}{5j\pi}\left\{e^{j2\pi(5f_s+f_c)t} - e^{-j2\pi(5f_s+f_c)t}\right\} + \\ &\vdots \end{aligned} \tag{3.8}$$

If the RF signal is modulated by the baseband signal, either analog or digital, the signal component appears in the harmonics. In conventional passive communication systems, all the sensor RF tag and the Reader/Writer share one subcarrier frequency for the tag-to-reader link. The Reader/Writer orchestrates the time division multiple access of sensor RF tags. The Reader/Writer usually uses the primal subcarrier by applying bandpass filter.

3.1.2 Multiple Subcarrier Communication System

In a multiple subcarrier communication system, each sensor RF tag is assigned a subcarrier frequency. If the number of sensor RF tags exceeds the available number of subcarriers, the Reader/Writer arbitrates the multiple access of sensor RF tag in a TDMA manner. In the following discussion, therefore, it presume the number of sensor RF tags is equal to the number of available subcarriers. The allocation of a subcarrier frequency to a sensor RF tag is assumed to be performed after the Reader/Writer inventories the available sensor RF tags with an existing multiple reading technique as shown in Fig.2.4.

According to the frequency spectrum of subcarrier communication theory in Eq.3.8, the original sensor RF tag signals are combined in the space and received by the Reader/Writer. An image of the interference distribution is shown in Fig.3.3.

The relationship between the original sensor RF tag signals and the received signals is

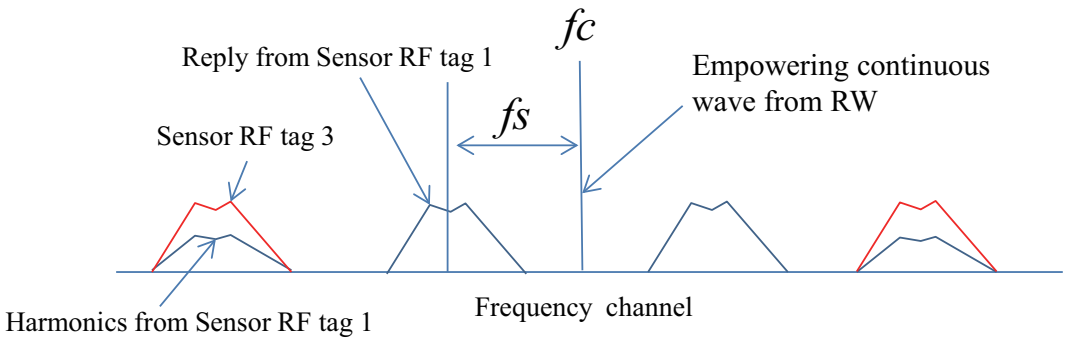

Figure 3.3: Harmonics interfere to other subcarriers in multiple subcarrier communications

represented as the following matrix equation.

$$\begin{Bmatrix} R_1 \\ R_2 \\ R_3 \\ \vdots \\ R_9 \\ \vdots \end{Bmatrix} = \begin{bmatrix} 1 & 0 & 0 & 0 & \cdots \\ 0 & 1 & 0 & 0 & \cdots \\ \frac{1}{3} & 0 & 1 & 0 & \cdots \\ \vdots & & & & \cdots \\ \frac{1}{9} & 0 & \frac{1}{3} & 0 & \cdots \\ \vdots & & & & \ddots \end{bmatrix} \begin{Bmatrix} T_1 \\ T_2 \\ T_3 \\ \vdots \\ T_9 \\ \vdots \end{Bmatrix} \tag{3.9}$$

In this equation, R_i represents the received signal on subcarrier channel i. T_i represents the original transmitted signal by sensor RF tag whose primal subcarrier channel is i. Even though the identification number of a subcarrier channel and that of a sensor RF tag are different in general, the sensor RF tag which transmits on subcarrier channel i referred as i^{th} sensor RF tag for brevity of the expression. Note that Eq.3.9 is a lower triangular matrix. Thus, the original sensor RF tag signals T_i can be recovered from the received signals R_i by a forward substitution as in Eq.3.10.

$$
\begin{aligned}
T_1 &= R_1 \\
T_2 &= R_2 \\
T_3 &= R_3 - \frac{1}{3}R_1 \\
T_9 &= R_9 - \frac{1}{9}R_9 - \frac{1}{3}R_3
\end{aligned}
\tag{3.10}
$$

3.2 Subcarrier Signal Model

As explained earlier, a subcarrier is produced by constant rate on/off keying of antenna impedance. Figure 3.4 shows the general backscatter signal from a sensor RF tag where the phase delay of subcarrier envelope ϕ is introduced. The backscatter signal is phase modulated with sensor signal x, there is a carrier phase delay Ψ_o, and modulation index m. Since the carrier phase delay and the signal phase delay can not be separable, the carrier phase shift denote collectively such that $\Psi = \Psi_o + x$.

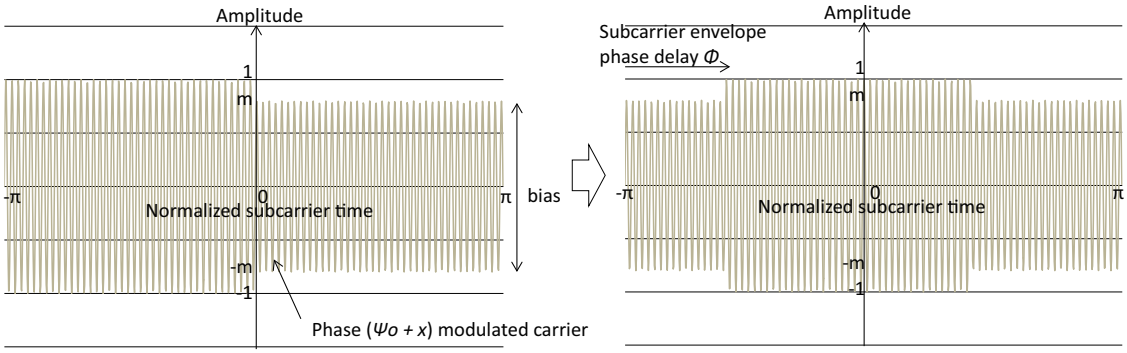

Figure 3.4: A typical subcarrier wave form. The envelop is changed with a constant rate toggling of an RF switch.

The frequency spectrum of the square waveform envelope $s_e(t)$ can be derived by applying the Fourier series expansion in Eq.3.11 where the time normalize from $-\pi$ to π with the

subcarrier period as shown in Fig.3.4.

$$f(t) = a_0 + \sum_{n=1}^{\infty}(a_n \cos nt + b_n \sin nt) \tag{3.11}$$

To derive coefficients a_0, a_n, and b_n of the Fourier series expansion, the integration region is divided into three zones. The bias component a_0 is derived from the following Eq.3.12.

$$\begin{aligned} a_0 &= \frac{1}{\pi}\left\{\int_{-\pi}^{-\pi+\phi} m\, dt + \int_{-\pi+\phi}^{\phi} 1\, dt + \int_{\phi}^{\pi} m\, dt\right\} \\ &= m + 1 \end{aligned} \tag{3.12}$$

A straightforward integration yields a_n and b_n as follows.

$$a_n = \frac{1-m}{n\pi}(\cos n\pi - 1)\sin n\phi \tag{3.13}$$

$$b_n = -\frac{1-m}{n\pi}(\cos n\pi - 1)\cos n\phi \tag{3.14}$$

The frequency response of the square waveform envelope $s_e(t)$ is shown in Eq.3.15.

$$\begin{aligned} s_e(t) &= m + 1 + \frac{2(1-m)}{\pi}\{\sin(t-\phi) + \frac{1}{3}\sin(3t-3\phi) + \frac{1}{5}\sin(5t-5\phi) + \cdots\} \\ &= m + 1 + \alpha \sum_{n=1,3,\cdots} \frac{1}{n}\sin(nt - n\phi) \end{aligned} \tag{3.15}$$

where

$$\alpha = \frac{2(1-m)}{\pi}. \tag{3.16}$$

The equations show that the higher harmonics accompany longer phase delay. This is the well known “linear group delay”.

It is also shown in Eq.3.15 that the harmonics of a subcarrier only appear in odd multiples of the primal subcarrier channel and higher harmonic produce less interference because of n in the denominator of Eq.3.15.

Note that the subcarrier signal is very small compared with the powering continuous wave because a subcarrier signal is fundamentally a reflection. Therefore, to obtain the maximum resolution of the modulated signal, the bias component of the signal is usually removed at the ingress of the receiver by applying a high pass filter (HPF). Denoting the subcarrier and the carrier angular velocities as ω_s and ω_c, respectively, the modulated subcarrier signal $S(t)$ can be written as below.

$$S(t) = \alpha \sum_{n=1,3,\cdots} \frac{1}{n} \sin(n\omega_s t - n\phi) \mathrm{e}^{j(\omega_c t + \Psi)} \tag{3.17}$$

The receiver downconverts the incoming subcarrier signal $S(t)$ by multiplying the carrier signal $\mathrm{e}^{-j\omega_c t}$ to yield the baseband signal $S_b(t)$ such that

$$\begin{aligned} S_b(t) &= \alpha \sum_{n=1,3,\cdots} \frac{1}{n} \sin(n\omega_s t - n\phi) \mathrm{e}^{j(\omega_c t + \Psi)} \mathrm{e}^{-j\omega_c t} \\ &= \alpha \sum_{n=1,3,\cdots} \frac{1}{n} \sin(n\omega_s t - n\phi) \mathrm{e}^{j\Psi} \end{aligned} \tag{3.18}$$

I and Q components after the down conversion are obtained as below.

$$\begin{aligned} I &= \alpha \sum_{n=1,3,\cdots} \frac{1}{n} \sin(n\omega_s t - n\phi) \cos\Psi \\ Q &= \alpha \sum_{n=1,3,\cdots} \frac{1}{n} \sin(n\omega_s t - n\phi) \sin\Psi \end{aligned} \tag{3.19}$$

As a result, S_b produces a straight line in the IQ plane, as in Fig.3.5, when there is a perfect subcarrier waveform. When the subcarrier has jitter, it may have a small orthogonal component which yields a flattened ellipse, as shown in the right figure of Fig.3.5.

The challenges in deriving harmonic replicas from a primal subcarrier signal, therefore, are summarized as follows.

- Handle ϕ and Ψ separately because the subcarrier phase delay ϕ in a harmonic replica shall be multiplied according to the order of harmonics to keep the linear group de-

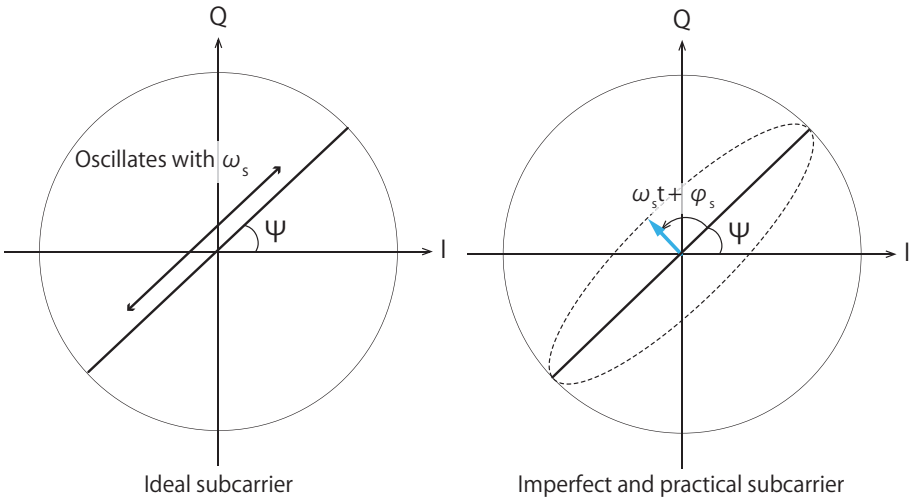

Figure 3.5: Real subcarrier signal with phase shift ϕ and Ψ. The real subcarrier signal moves at $n\omega_s t - n\phi$ with initial incline Ψ. Note that the subcarrier signal crosses the 0 point.

lay, while Ψ stays the same in all the harmonic replicas. For example, for n-th order harmonics $n\omega_s$ and the delay angle shall be $n\phi$, as shown in Eq.3.18.

- Derive the amplitude of primal signal to yield the predefined amplitude degradation term $\frac{1}{n}$ in Eq.3.18 while the amplitude of primal subcarrier fluctuates as the IQ components move along an ellipse or a straight line.

In the following, a solution to overcome the above two problems to establish basic demodulation process in MSMA is introduced. A method is proposed to derive the carrier phase shift Ψ in the first section. The next section proposes a method to use the Hilbert transformation and inverse Hilbert transformation for harmonic replica generation.

3.3 Estimation of Carrier Phase Delay Ψ with Recursive Least Square Method

Obtaining Ψ by decomposing the primal subcarrier signal into the amplitude and the phase angle does not properly work because by doing so, it ends up with two phase angle candidates

which are mutually separated by π radians. To solve this problem, a regression analysis apply with a recursive least square (RLS) of the primal subcarrier with an assumption that the subcarrier signal in IQ plane can be approximated by the following linear equation

$$Q - \tan \Psi I = 0 \tag{3.20}$$

A regression analysis with $j-1$ set of IQ data yields the optimal $\tan \Psi$ such that

$$\tan \Psi_{j-1} = \frac{\sum_{i=1}^{j-1} I_i Q_i}{\sum_{i=1}^{j-1} I_i I_i} \tag{3.21}$$

Suppose the past $j-1$ set of IQ signals measurements and estimated $\tan \Psi_{j-1}$ are already available. With a new set I_j, Q_j, $\tan \Psi_j$ can update with a forget factor η such that

$$\tan \Psi_j = \frac{I_j Q_j}{I_j^2} + \eta \tan \Psi_{j-1} \tag{3.22}$$

3.4 Replica Generation with Hilbert and Inverse Hilbert Transformations

Because the amplitude of the measured subcarrier signal fluctuates in time, the amplitude of the signal should be derived and be adjusted to produce harmonics replicas. For this purpose, an analytic signal of subcarrier is introduce. The analytic signal is generated orthogonal to the real subcarrier signal and whose amplitude fluctuates to keep the instantaneous envelope constant when it is combined with the the real subcarrier. The process to generate an analytic signal from a real signal is known as a Hilbert filter or Hilbert transformation. IQ components

of analytic signal of the subcarrier, denoted as $\bar{I}, \bar{Q}$, are given as follows.

$$\begin{aligned} \bar{I} &= -\alpha \cos(\omega_s t - \phi) \sin \Psi \\ \bar{Q} &= \alpha \cos(\omega_s t - \phi) \cos \Psi \end{aligned} \tag{3.23}$$

The combined real and analytic signal, denoted as the augmented subcarrier signal Z, rotates with subcarrier frequency keeping the instantaneous amplitude constant.

$$Z = I + \bar{I} + j\left\{Q + \bar{Q}\right\} \tag{3.24}$$

Since Ψ stays the same when a harmonic produce, the augmented signal is counter-rotate by

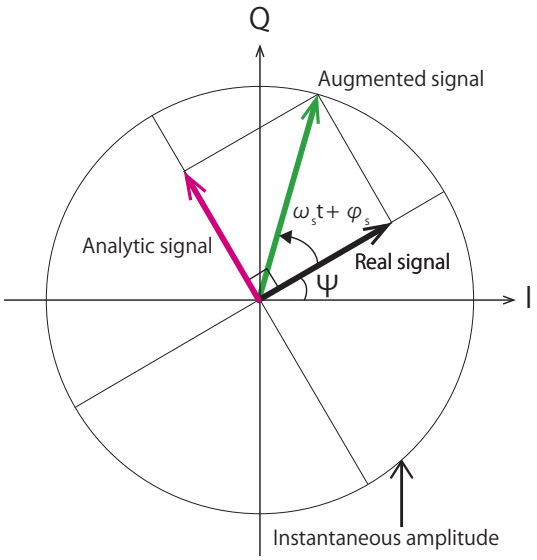

Figure 3.6: Real signal and its analytic signal produced by Hilbert transformation together form the augmented signal which rotate with an instantaneous amplitude.

Ψ to obtain the following circle.

$$\begin{aligned} Z_s &= Ze^{-j\Psi} \\ &= \alpha \sin(\omega_s t - \phi) + j\alpha \cos(\omega_s t - \phi) \end{aligned} \tag{3.25}$$

This way, harmonics of the augmented signal can be produced, denoted as augmented harmonics, simply by multiplying the phase angle obtained, for example, by a phase locked loop (PLL) and applying appropriate scaling according to the order of harmonics, as shown in Fig.3.7. The harmonic replica is obtained by adding the carrier phase delay Ψ and projecting

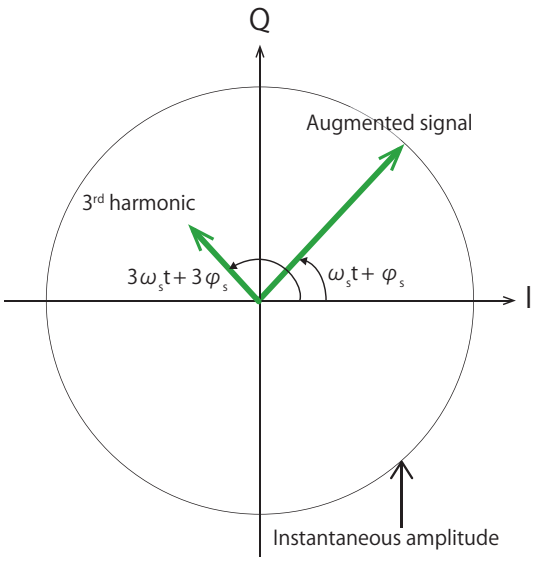

Figure 3.7: Augmented harmonic can be produced by multiplying the phase angle of the augmented signal by the order of the harmonic and adjusting the amplitude dividing by the order of the harmonic.

the augmented harmonics to the Ψ plane. Since this projection provides the inverse operation of Hilbert transformation, this projection is referred to as Inverse Hilbert Transformation. When an augmented harmonics denote as

$$\boldsymbol{r} = \boldsymbol{r_r} + \boldsymbol{j r_i} \tag{3.26}$$

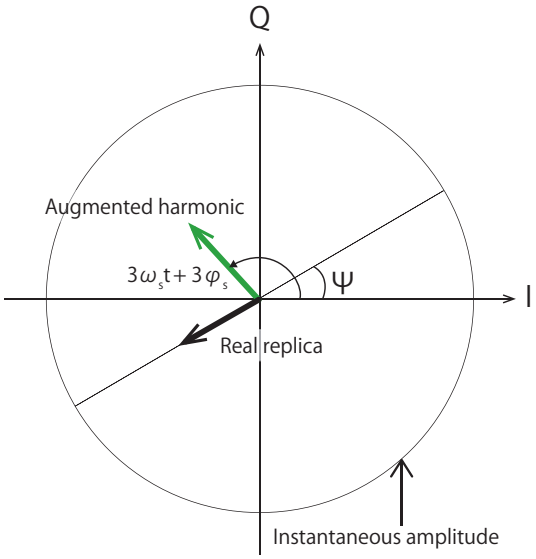

Figure 3.8: Real harmonic replica can be obtained by projecting the augmented harmonic on the original Ψ plane.

and the unit vector of the carrier phase plane as $\cos\Psi + j\sin\Psi$, the Inverse Hilbert transformation of r, $H^{-1}(r)$, can be concisely represented by the following linear transformation.

$$\begin{aligned} H^{-1}(r) &= (r_r\cos\Psi + r_i\sin\Psi)(\cos\Psi + j\sin\Psi) \\ &= \begin{bmatrix} \cos\Psi\cos\Psi & \cos\Psi\sin\Psi \\ \cos\Psi\sin\Psi & \sin\Psi\sin\Psi \end{bmatrix} \begin{Bmatrix} r_r \\ jr_i \end{Bmatrix} \end{aligned} \tag{3.27}$$

3.5 Harmonics Rejection

Let us first consider a simple case, where there is a primal subcarrier and a harmonic from another subcarrier interfering with the primal subcarrier as shown in Fig.3.9. The carrier phase delay, Ψ_1, Ψ_2 of each subcarriers are independent. The observed signal in the subcarrier channel of sensor RF tag 2 is the superposition of those two subcarriers. When the replica of the harmonics from the primal subcarrier signal of sensor RF tag 1 is produced, the method can recover the primal signal of sensor RF tag 2 by subtracting the replica from the observed signal.

Next, a case is considered where nine sensor tags exist. The nine sensor tags use differ-

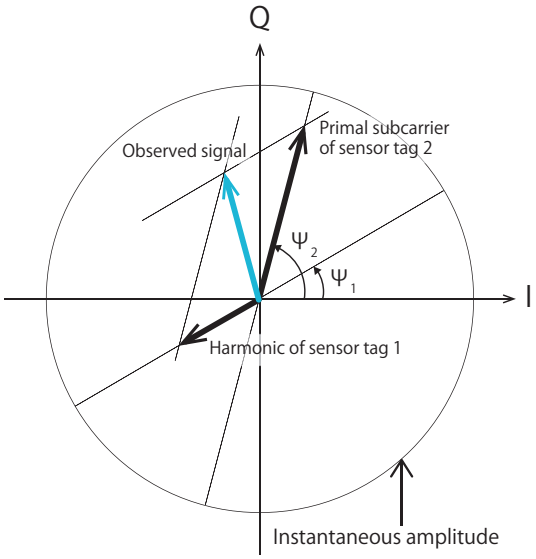

Figure 3.9: The harmonic from sensor RF tag 1 is interfering with the primal subcarrier from sensor RF tag 2. The synthesized vector will be observed at the subcarrier channel of sensor RF tag 2.

ent subcarrier channels from f_1 to f_9. For the simplicity, it is assumed sensor RF tag i uses subcarrier channel i without loss of generality. Each subcarrier is assumed to be modulated with an analog sensor stream. Because of the nature of the subcarrier signal, some harmonics of a subcarrier fall into the other sensors bandwidth such that each subcarrier produces harmonics at odd number multiples of the subcarrier frequency. Since the method can remove the contribution of the envelope and carrier delay with Hilbert and inverse Hilbert transformations explained in the previous section, the modulated subcarrier signal $A_i e^{j\Psi_i}$ as the transmitted signal and R_i as the received signal is considered only, where i denotes i-th subcarrier frequency.

$$\begin{Bmatrix} R_1 \\ R_2 \\ R_3 \\ \vdots \\ R_9 \end{Bmatrix} = \begin{bmatrix} \sin(\omega_1 t - \phi_1) & 0 & 0 & \cdots & 0 \\ 0 & \sin(\omega_2 t - \phi_2) & 0 & \cdots & 0 \\ \frac{1}{3}\sin(3\omega_1 t - 3\phi_1) & 0 & \sin(\omega_3 t - \phi_3) & \cdots & 0 \\ \vdots & & & \ddots & \vdots \\ \frac{1}{9}\sin(9\omega_1 t - 9\phi_1) & 0 & \frac{1}{3}\sin(3\omega_3 t - 3\phi_3) & \cdots & \sin(\omega_9 t - \phi_9) \end{bmatrix} \begin{Bmatrix} A_1 e^{j\Psi_1} \\ A_2 e^{j\Psi_2} \\ A_3 e^{j\Psi_3} \\ \vdots \\ A_9 e^{j\Psi_9} \end{Bmatrix} \tag{3.28}$$

Note that Eq.3.28 is a lower triangular matrix and every instantaneous component in the matrix can be measured and sequentially computed with the procedure in Section 3.6. Therefore, after obtaining the modulated subcarrier signals of sensor RF tag 1, all the interferences can remove caused by sensor RF tag 1 as in Eq.3.29. After this harmonics rejection, the each separated subcarrier is demodulated to obtain its original signal.

$$\begin{Bmatrix} R_2 \\ R_3 - \frac{A_1 e^{j\Psi_1}}{3}\sin(3\omega_1 t - 3\phi_1) \\ \vdots \\ R_9 - \frac{A_1 e^{j\Psi_1}}{9}\sin(9\omega_1 t - 3\phi_1) \end{Bmatrix} = \begin{bmatrix} \sin(\omega_2 t - \phi_2) & 0 & \cdots & 0 \\ 0 & \sin(\omega_3 t - \phi_3) & \cdots & 0 \\ \vdots & & \ddots & \vdots \\ 0 & \frac{1}{3}\sin(3\omega_3 t - 3\phi_3) & \cdots & \sin(\omega_9 t - \phi_9) \end{bmatrix} \begin{Bmatrix} A_2 e^{j\Psi_2} \\ A_3 e^{j\Psi_3} \\ \vdots \\ A_9 e^{j\Psi_9} \end{Bmatrix} \tag{3.29}$$

The number of interfering channels in MSMA is at most five at channel 45 when total fifty subcarrier channels are available, as shown in Fig.3.10. When it is assumed all the subcarrier

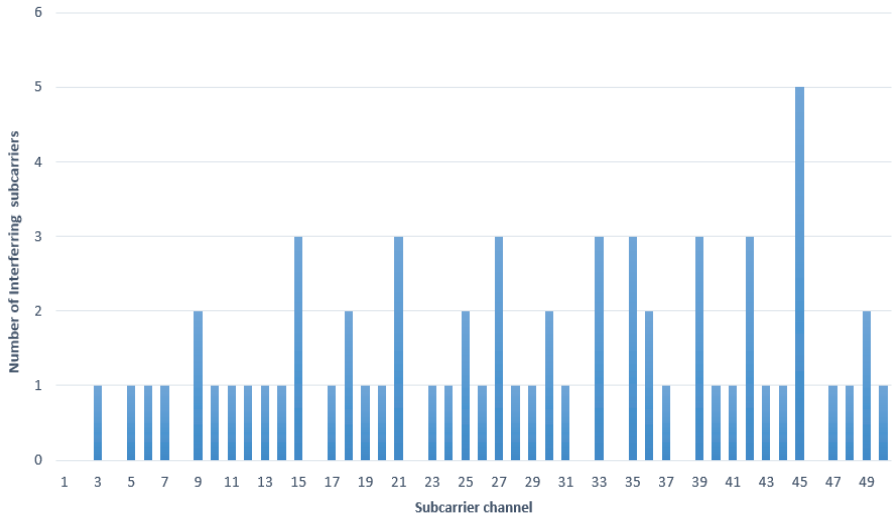

Figure 3.10: Distribution of the number of interfering subcarriers in subcarrier channel. Subcarrier channel 1 denotes the closest channel to the powering frequency.

signals have the same power, which is the case when all the sensor tags are located at the same distance from the Reader/Writer, the carrier to interference ratio (CIR) of fifty subcarrier channels are calculated as in Fig.3.11, where CIR of no interfered channel, such as channel

1 and 2, is denoted as 20dB. It is shown that the total CIR is not affected very much by the subcarriers which have large frequency separation from the victim channel. Take channel 45 as an example, the total CIR is slightly less than 8dB, which is equivalent to channel 15, even though five subcarriers interfere at channel 45, while at channel 15 is three.

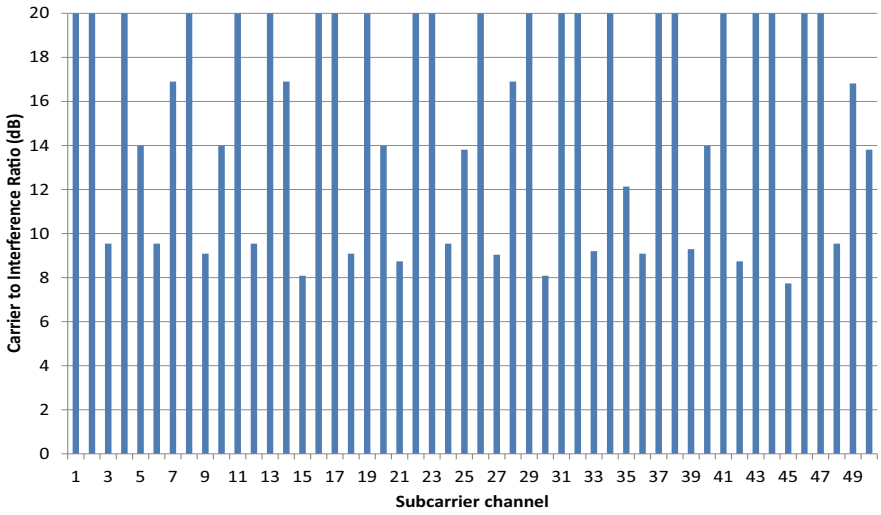

Figure 3.11: Total CIR is dominated by close subcarriers. Even if the number of interfering subcarriers is large, the total CIR is not degraded very much.

3.6 Evaluation

3.6.1 Evaluation Setup

An MSMA simulator is implemented with Simulink to verify the fundamental characteristics of MSMA and also developed an experiment system with USRP2920 and LabVIEW. The overview of the demodulation process in both the simulator and the experimental of system for nine subcarrier channels is shown in Fig.3.12. The simulated signal and received signal

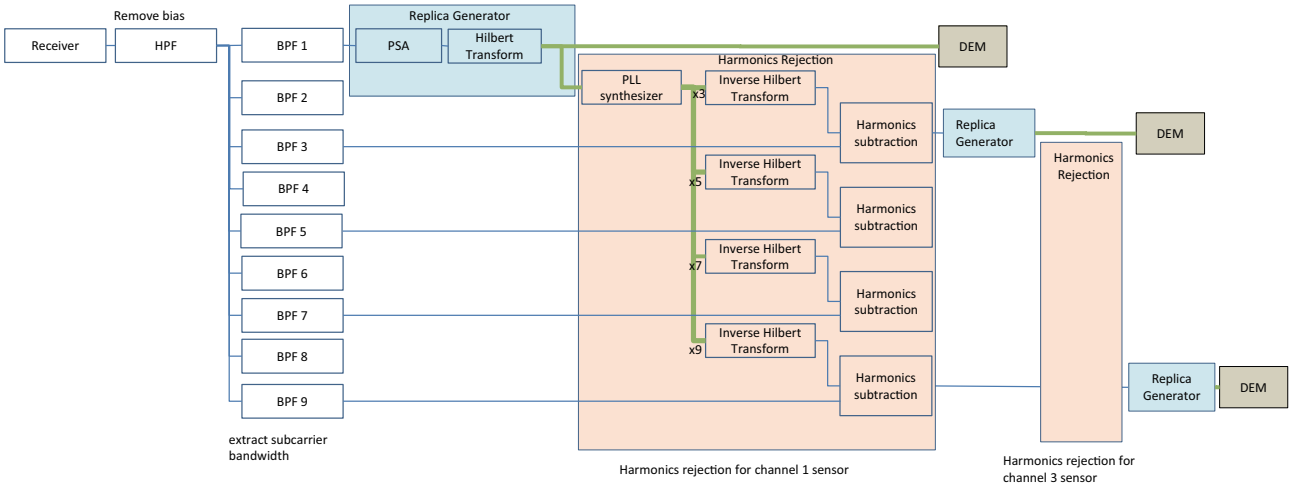

Figure 3.12: MSMA Harmonics Rejection Receiver is constructed both in Simulink and Experimental System.

by USRP2920 first passes through HPF in order to remove the bias signal to yield the maximum resolution of subcarrier signal. After the HPF, each subcarrier channel is filtered out by Band Pass Filters (BPF). The carrier phase delay of the filtered subcarrier signal is estimated by a regression analysis with an RLS, then an augmented signal is generated with Hilbert transformation and constant instantaneous amplitude is acquired. Next the augmented signal is processed by PLL to obtain the frequency of the primal subcarrier signal. Based on Eq.3.18, augmented n-th order harmonics are generated with the frequency and instantaneous amplitude which are obtained by multiplying the primal subcarrier frequency and dividing the instantaneous amplitude of the primal subcarrier signal by n respectively. In order to obtain

an n-th order real harmonics replica, augmented n-th order harmonics are processed by inverse Hilbert transform, taking into consideration the estimated carrier phase delay. Finally the interference is rejected by subtracting the real harmonics replica from the interfered subcarrier channel. Sequentially processing the above procedure based on the matrix in Eq.3.28, the mutual interferences can be rejected.

The simulation on Simulink is carried out to verify the proposed fundamental MSMA demodulation process. The parameters used for the simulations are listed in Table 3.1. For the

Table 3.1: The simulation parameters

Simulation Parameter	**Value**	
Subcarrier frequency	sensor RF tag 1	20kHz
	sensor RF tag 2	60kHz
	sensor RF tag 3	180kHz
Sensor signal(sin wave)	sensor RF tag 1	2kHz
	sensor RF tag 2	1kHz
	sensor RF tag 3	500Hz

simulation concurrent sensor data streaming and demodulation with 3 sensor RF tags whose harmonics are mutually interfering are considered. The mutually interfering subcarrier frequencies for each sensor RF tag are intentionally selected to evaluate the effect of our proposed interference rejection process. The harmonic of sensor RF tag 1 is interfering with the primal subcarrier of sensor RF tag 2 and harmonics of sensor tags 1 and 2 are interfering with the primal subcarrier of sensor RF tag 3. In this simulation, all the harmonics of sensor RF tag 1 is calculated and rejected at first, then sensor RF tag 2's primal subcarrier is recovered. Finally the harmonics of sensor RF tag 2 is calculated and the sensor RF tag 3's primal subcarrier is recovered.

For the experimental evaluation, a sensor model is developed with a phase modulator and RF switch as shown in Fig.3.13. The RF switch (PE42421SCAA-Z) is controlled by a TI MSP430. The antenna impedance of the sensor RF tag is changed by switching the route to open ended or terminated and the subcarrier signal is generated. The sinusoidal waveform as

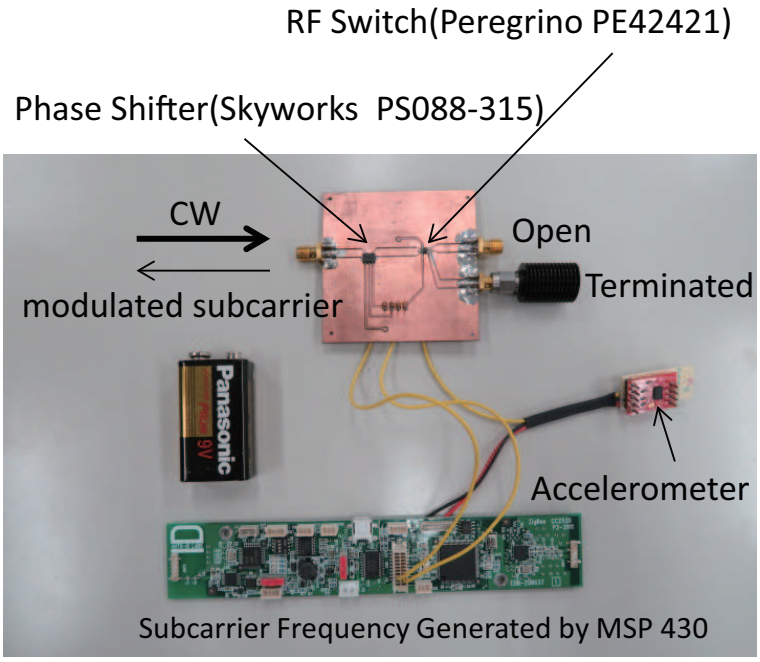

Figure 3.13: A sensor model developed for the experimental verification of MSMA. Though an accelerometer is connected and it is feasible to obtain vibrational data, sinusoidal waveform generated by function generator is input as a sensor signal for this experiment in order to obtain continuous signal.

a sensor signal from the function generator is modulated onto the outgoing subcarrier signal by a phase shifter (Skyworks PS088-315). Each sensor signal frequency is the same as the parameters shown in Table 3.1.

The sensor model is not batteryless at this moment. But considering there is an experimental platform to use MSP430 as batteryless sensor RF tag [41], the very low power consumption commercial MEMS accelerometer [42] and a commercial passive RF tag with accelerometer function [16], it can be said that a passively powered sensor RF tag could be build with current LSI process and sensor technology.

Figure 3.14 shows the block diagram of the experiment setup. The signal generator generates a CW at 915MHz as a transmitted signal from Reader/Writer. The carrier signal is backscattered by the sensor RF tag and the subcarrier signal is combined and received by USRP2920. The USRP2920 is connected to a PC through Gigabit Ethernet cable, and IQ data

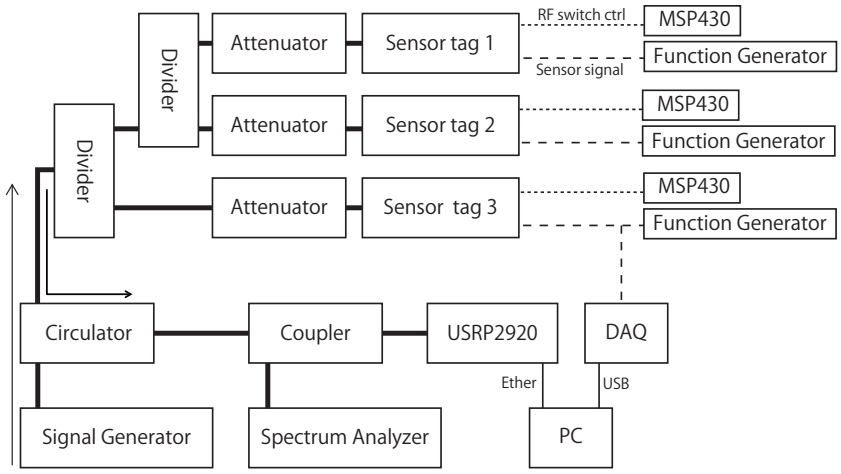

Figure 3.14: Experiment setup block diagram. All components are connected with coaxial cable except a PC, MSP430s, and function generators for accurate adjustment of the signal level.

are processed by a Virtual Instrument (VI) in LabVIEW. Each sensor signal from the function generator is also measured on the VI via NI USB-6009(DAQ in Fig.3.14) and compared with the demodulated signal. The process of the VI is based on Fig.3.12.

Configurations for the subcarrier frequency and the sensor signal of each sensor RF tag are identical to the simulation. At the ingress of each sensor RF tag, a variable attenuator is installed to change the Carrier to Interference Ratio(CIR) that emulates the distance difference between each sensor RF tag and a Reader/Writer.

3.6.2 Result of Simulations and Experiments

In order to quantitatively evaluate the result of simulations and experiments, the correlation coefficients are derived and compared between the demodulated sensor signal and the original sensor signal at respective CIR environment as shown in Fig.3.15. CIR 0 dB represents an environment in which power of the interfering signals from sensor tags 1 and 2 and the power of the desired subcarrier signal from sensor RF tag 3 are same. Even in case of CIR 0 dB, the correlation coefficients in both simulation and experiment are over 0.98. When it comes to CIR

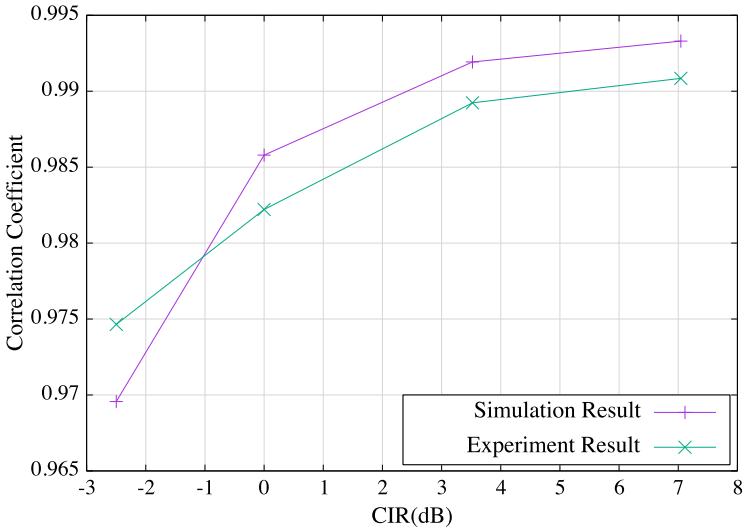

Figure 3.15: A comparison of correlation coefficients derived from simulation result and experiment results corresponding to the CIR change.

7 dB the correlation coefficients are improved over 0.99 in both case. Both in the simulation and the experiment, the environment that 2 harmonics are interfering with the primal subcarrier of sensor RF tag 3. The two harmonics interfering condition is the worst case when there are less than 14 sensors in the reading area, because the minimum number of sensor tags when there are 3 harmonics interfering can be calculated as 14 based on the lower triangular matrix in Eq.3.28 and Fig.3.10. Therefore it can be said that the proposed demodulation process is capable of concurrently demodulating sensor data from at least 14 sensors. In addition, the quality improvement of the recovered signal according to the rise of CIR indicates that the subcarrier frequency allocation scheme has an important role in MSMA.

Let us introduce a part of the original signal and the demodulated signal from sensor RF tag 3 in the experiment. Figure 3.16 shows the comparison of those signals at different CIR (0 dB, 7 dB). Even though small fluctuations are observed in the case of CIR 0 dB on the demodulated signal, still it shows good approximation to the original signal. In the case of CIR 7 dB, there is much less fluctuation compared with the case of CIR 0 dB.

The contribution of the harmonic rejection method depends on the original CIR. The CIR

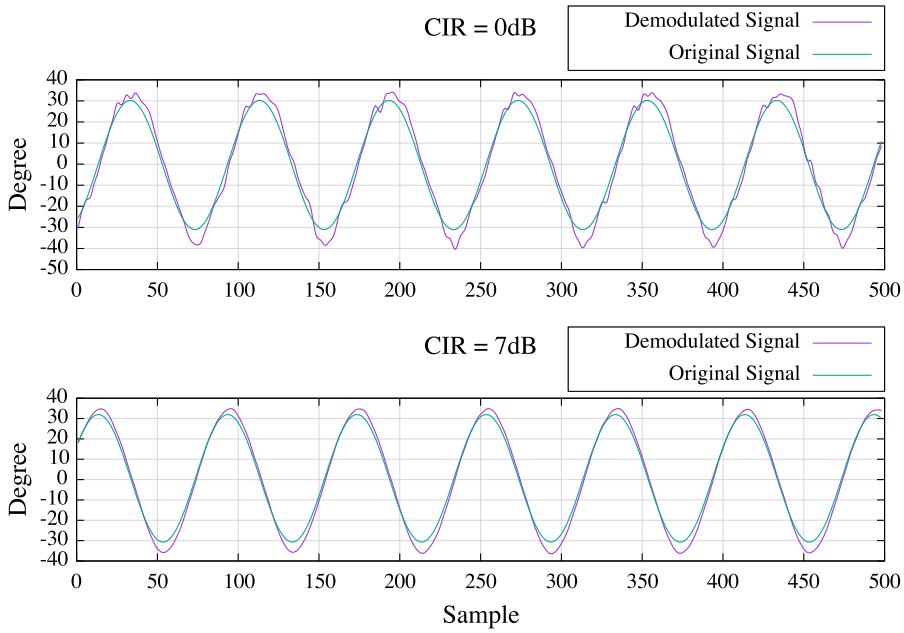

Figure 3.16: Concurrently received and demodulated signal from sensor RF tag 3 is compared with its original signal from function generator.

of a sensor RF tag depends on its allocated subcarrier frequency and the distance it is located from the Reader/Writer. In Fig.3.15, the performance of harmonic rejection method is shown for above -3 dB because the CIR can be improved with the subcarrier allocation schemes. Figure 3.17 shows an example of varying range of CIR when fifty sensor RF tags are randomly distribuited in the area of 10 meter radius and the subcarriers are allocated with the random allocation and heuristic allocation method. It is shown that after the allocation CIR can be assumed above 0 dB for every sensor RF tags.

3.7 Summary

Concurrent sensor data streaming from batteryless wireless sensors can be realized by using the proposed multiple subcarrier multiple access (MSMA). Because of the minimum functional requirements on sensors, concurrent sensor data streaming entails mutual interference.

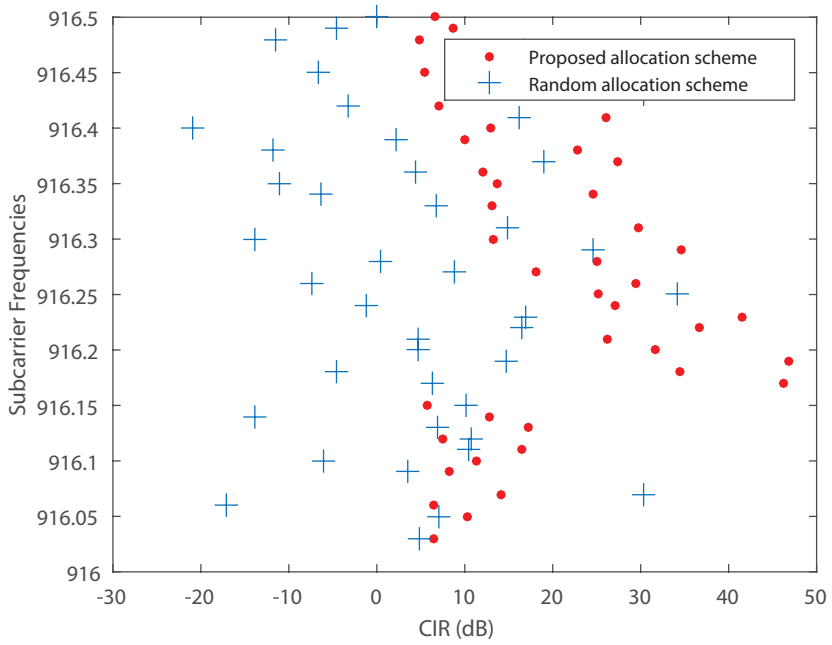

Figure 3.17: CIR range can be improved by the proposed assignment method

Yet, the mutual interference can be accurately rejected with the harmonics rejection receiver proposed herein. The challenges of the receiver reside in the careful handling of the phase delay of the subcarrier envelop and the carrier signal. The harmonics rejection receiver solves this problem by handling those delays in an augmented IQ signal which is produced by Hilbert transformation and projecting it back to the real IQ signal by a mathematical treatment which referred as inverse Hilbert transformation. By successively subtracting the harmonics replica from the received signal, the original sensor data streaming can accurately recover at the receiver. The achieved accuracy is confirmed, both with simulations and experiment, to be above 0.98 cross-correlation even when the CIR before the harmonics rejection is 0 dB.

Chapter 4

Subcarrier Allocation in MSMA

4.1 Introduction

Multiple subcarrier passive communication is a new research area which enables a type of frequency division multiple access with wireless and batteryless sensor RF tags just by implementing RF switches to produce dedicated subcarriers. Since the mutual interference among the subcarriers is unevenly distributed over the frequency band, careless allocations of subcarrier frequencies may result in degraded system performance and inefficient use of the frequency resource.

This chapter is divided into two sections based on the required bandwidth by the sensor RF tags. Section 4.2 explains the fixed bandwidth subcarrier allocation and setup of comparative analysis on various subcarrier allocation schemes using MATLAB simulation. Section 4.3 studies the subcarrier allocation problem when the sensor RF tags requires variable bandwidth subcarrier.

4.2 Fixed Bandwidth Subcarrier Allocation

4.2.1 Problem Statement and System Model

The subcarrier frequency allocation to sensor RF tags in accordance with their signal quality is influential to the total communication capacity. To evaluate the communication capacity, four subcarrier frequency allocation schemes are explained and examined in the following section. The accessibility fairness for the four schemes is also examined.

Let us consider that there are N sensor RF tags and one Reader/Writer. The available bandwidth of the system is denoted as W. Each subcarrier frequency consumes a constant bandwidth B Hz, thus $W = BN$. Figure 4.1 shows the relationship between the central frequency f_c, the subcarrier frequency f_j, W, N and B. At any given time instance, the Reader/Writer communicates simultaneously with each sensor RF tag. The communication capacity of the whole system is evaluated using Shannon's theorem [43] as in Eq. 4.1 where c_i denotes the communication capacity of i^{th} sensor RF tag. Please note that it does not mean to use adaptive modulation and forward error correction in the multiple subcarrier communication system. It is an index to evaluate communication capacity in a general way.

$$c_i = B \log_2 (1 + \mathrm{SINR_i}) \tag{4.1}$$

$\mathrm{SINR_i}$ stands for Signal-to-Interference-Noise Ratio of the i^{th} sensor RF tag. The free space loss is employed here but any propagation model can be applied such as extended HATA SRD [44]. Also it is assumed that, when a sensor RF tag backscatters the signal, 90% of signal power attenuated.

For simplicity, it is assumed that the sensor RF tag resides on subcarrier frequency i is called i^{th} sensor RF tag, i^{th} sensor RF tag is placed at distance r_i away from the Reader/Writer operating on the fundamental subcarrier frequency (i) generates the harmonic component at subcarrier frequency (j) with the power spectrum as shown in Eq. 4.2, where H_{ij} represents the

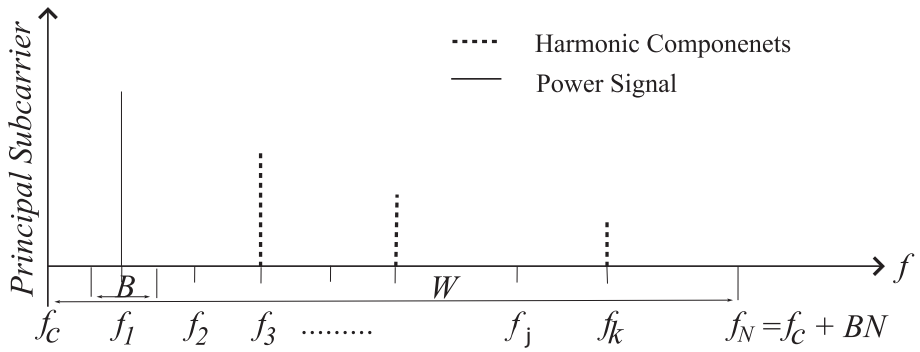

Figure 4.1: Relationship among f_c, W, B and N.

power of harmonic components generated by the i^{th} sensor RF tag onto the specified subcarrier frequency j. The signal power S_i depends on distance (r_i) and subcarrier frequency i, on which sensor RF tag backscatter, f_i, such that $f_c < f_i < (f_c + W)$. More specifically, it depends on the difference between subcarrier and central frequency ($f_i - f_c$), i.e. further away from the central frequency a sensor RF tag is operated, Reader/Writer receives less signal power.

$$H_{ij} = \begin{cases} i\frac{S_i}{j} & \text{if}(i = mj, m = 3, 5, 7 \cdots) \\ 0 & \text{if}(i \neq mj) \end{cases} \tag{4.2}$$

It is shown that a given subcarrier f_k produces interference harmonics at $f_{3k}, f_{5k}, ...$ For example, f_1 produces interference harmonics at $f_3, f_5, ...$ whereas f_7 produces interference harmonics at $f_{21}, f_{35}, f_{49}, ...$ Figure 4.2 shows an example of harmonic interference when all the subcarrier bandwidth is fixed.

A given subcarrier f_j may receive interference from several other subcarriers f_i (where $i < j$) with the power as shown in Eq. 4.2. The total interference power is the sum of all H_{ij} as shown in Eq. 4.3.

$$H_j = \sum_{i=1}^{\lfloor j/3 \rfloor} H_{ij} \tag{4.3}$$

The noise temperature (T) of a Reader/Writer is assumed to be constant which is given by

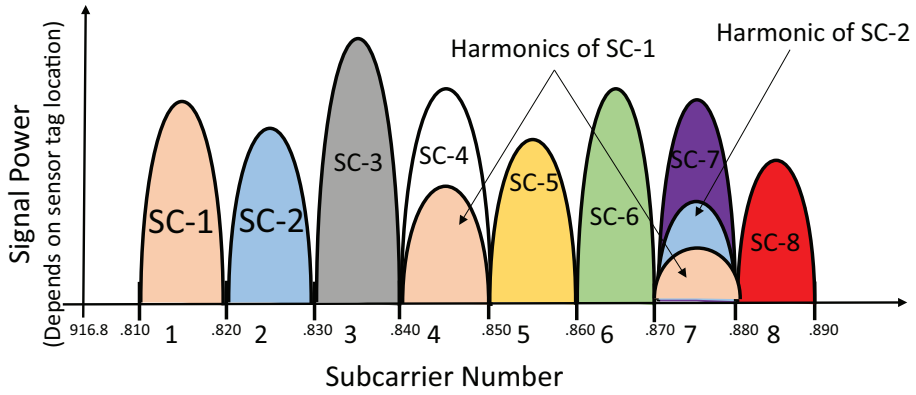

Figure 4.2: Harmonics interfere to other subcarriers, when subcarrier bandwidth is fixed

$n_T = kTB$ where n_T, k, T, B represents total noise power (W), the Boltzmann constant (J/K), temperature (K) and bandwidth (Hz), respectively. The constant n_T = -130 dBm is used.

$SINR_i$ denoted SINR value for each sensor RF tag allocated subcarrier frequency f_i located at distance r_i from the Reader/Writer, receiving signal power S_i, interference H_i and thermal noise n_T. Then the total Shannon capacity of all sensor RF tags can be obtained by simply adding them as in Eq. 4.4.

$$\begin{aligned} C &= \sum_{i=1}^{N} c_i = \sum_{i=1}^{N} B \log_2(1 + SINR_i) \\ &= \sum_{i=1}^{N} B \log_2(1 + \frac{S_i}{H_i + n_T}) \end{aligned} \tag{4.4}$$

4.2.2 Proposed Allocation Schemes

In this section, four subcarrier allocation schemes are introduced: Random Allocation Scheme (RAS), Nearest Tag Nearest Subcarrier (NTNS), Farthest Tag Nearest Subcarrier (FTNS), Mixed Allocation Scheme (MAS) for sensor RF tags.

4.2.2.1 Random Allocation Scheme (RAS)

Algorithm 1 Random Allocation Scheme

1: T is the set of sensor RF Tags which yet to be assigned to a subcarrier.
2: let i denotes the sensor RF tag index and j denotes the subcarrier index.
3: S_N is the total number of subcarriers.
4: j = 0 ;
5: **while** j $\neq S_N$ **do**
6: Choose randomly any sensor RF tag from the set T, T_i.
7: Assign subcarrier S_j to T_i and delete T_i from the set T.
8: $j \leftarrow j + 1$;
9: **end while**

RAS scheme picks a sensor RF tag randomly and assign the first subcarrier to it, then picks another sensor RF tag randomly and assigns the second subcarrier and so on. Algorithm 1 shows the pseudo code of RAS.

4.2.2.2 Nearest Tag Nearest Subcarrier (NTNS)

First, the sensor RF tags are arranged in a list based on the distance from the Reader/Writer. The algorithm picks the first sensor RF tag from the list and assigns it to first subcarrier, then picks the second sensor RF tag and assigns it to the second subcarrier and so on. Pseudo code for NTNS is presented in Algorithm 2

Algorithm 2 Nearest Tag Nearest Subcarrier

1: Arrange all the sensor RF tag in a list in increasing order based on the distance far from the Reader/Writer.
2: let i denotes the sensor RF tag index in the list and j denotes the subcarrier index.
3: lets S_N is the total number of subcarriers.
4: j = 0;
5: **while** j $\neq S_N$ **do**
6: Pick the RF tag T_i from the list; {one by one from the list. $i = 1, 2, 3...N$}
7: Assign subcarrier (S_j) to T_i and delete from the list;
8: $j \leftarrow j + 1$;
9: **end while**

4.2.2.3 Farthest Tag Nearest Subcarrier (FTNS)

FTNS is basically the reverse of NTNS, the scheme picks the last sensor RF tag from the list and assigned it to the first subcarrier and so on presented in Algorithm 3.

Algorithm 3 Farthest Tag Nearest Subcarrier

1: Arrange all the sensor RF tag in a list in increasing order based on the distance far from the Reader/Writer.
2: lets S_N is the total number of subcarriers.
3: let i denotes the sensor RF tag index in the list and j denotes the subcarrier index.
4: $j = S_N$;
5: **while** $j \neq 0$ **do**
6: Pick the sensor RF tag T_i from the list; {one by one from the list. $i = 1, 2, 3...N$}
7: Assign subcarrier (S_j) to RF Tag T_i and delete from the list;
8: $j \leftarrow j - 1$;
9: **end while**

4.2.2.4 Mixed Allocation Scheme (MAS)

An another allocation scheme which is basically the combination of NTNS and FTNS is called Mixed allocation scheme presented on Algorithm 4. It can be noted that interference or harmonic components are generated only from subcarrier number 1 to $\lfloor N/3 \rfloor$, where N is the total number of subcarriers, equals to the number of sensor RF tags. To reduce the power

of harmonic components the scheme assigned subcarrier from 1 to $\lfloor N/3 \rfloor$ to sensor RF tags which are farthest away from the Reader/Writer and then the scheme assigned the sensor RF tags which is near to Reader/Writer from subcarrier number $\lfloor \frac{N}{3} \rfloor + 1$ to N, which increases the $SINR$ of RF tags which implies better capacity.

Algorithm 4 Mixed Allocation Scheme

1: Arrange all the tag T in a list in increasing order based on the distance far from the Reader/Writer.
2: let i denotes the sensor RF tag index in the list and j denotes the subcarrier index.
3: lets S_N is the total number of subcarriers.
4: $i = N$ and $j = 1$;
5: **while** $j \leq \lfloor N/3 \rfloor$ **do**
6: Pick the tag T_i from the list; $\{i = N, N-1,...\lfloor 2N/3 \rfloor\}$.
7: Assign subcarrier (S_j) to tag T_i and delete from the list; $\{j = 1, 2, 3,...\lfloor N/3 \rfloor\}$.
8: $i \leftarrow i - 1$;
9: $j \leftarrow j + 1$;
10: **end while**
11: $i = 1$ and $j = \lfloor N/3 \rfloor + 1$;
12: **while** $j \leq N$ **do**
13: Pick the tag T_i from the list; $\{i = 1, 2,...\lfloor 2N/3 \rfloor\}$.
14: Assign subcarrier (S_j) to tag T_i and delete from the list; $\{j = \lfloor N/3 \rfloor + 1, \lfloor N/3 \rfloor + 2....N\}$.
15: $i \leftarrow i + 1$;
16: $j \leftarrow j + 1$;
17: **end while**

4.2.3 Simulation Results and Analysis

The proposed subcarrier allocation schemes are simulated in MATLAB and their performance are evaluated. The sensor RF tags are uniformly distributed in a 10 m $\times$ 10 m square area in random fashion and the Reader/Writer is located at the center. Monte Carlo simulation runs for 100 trials to derive the average. The simulation parameters are listed in Table 4.1. Initially the allocation schemes are analyzed to see how average communication capacity is affected

without the harmonic rejection method. The average communication capacity is defined as the ratio of sum of communication capacity of all sensor RF tags and the total number of sensor RF tags.

Table 4.1: Simulation Setup

Simulator	Matlab
Subcarrier Bandwidth	1 KHz
Network Layout	Single-Cell with Omni-directional Antenna
No. of Subcarrier	Equal to Number of Tags
Total No. of Devices	10, 20, 30, 40, 50
Tag Position	Constant in Square area
Reader/Writer Antenna Gain	0dBi (Omni Directional)
Reader/Writer Transmitting Power	1 W

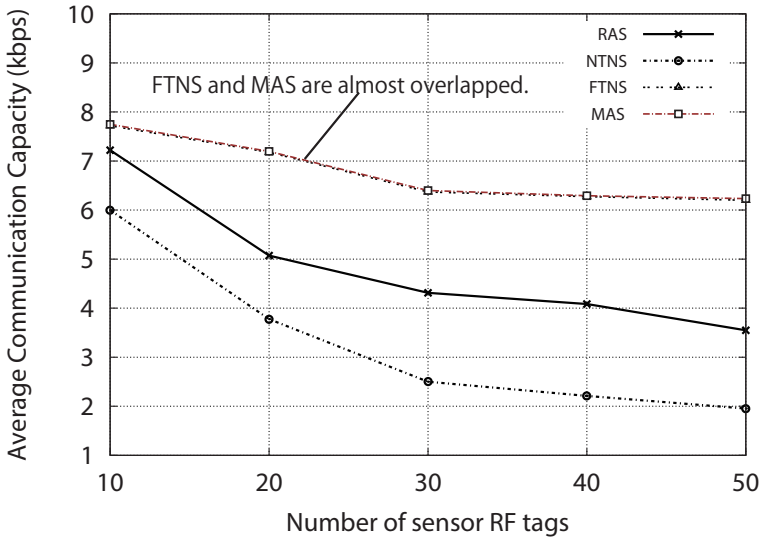

Figure 4.3: Average communication capacity comparison for different allocation schemes

Figure 4.3 shows the average communication capacity of four allocation schemes with varying numbers of sensor RF tags. All schemes show decreasing average communication capacity as the number of sensor RF tags increases, because more interference and noise are

generated in a band. The comparison of allocation schemes for a given number of devices reveals that NTNS achieves the lowest average communication capacity. This is because placing strong signal sensor RF tags on the closest subcarrier channels results in the worst interference to other subcarrier channels, thereby degrading the overall system communication capacity. Please note that FTNS and MAS are almost overlapped. A small improvement over FTNS is done by MAS scheme whereby subcarrier channels which have odd multiples outside the given band ($> f_{N/3}$), and hence no interference on other subcarrier channels are allocated in NTNS manner to improve signal.

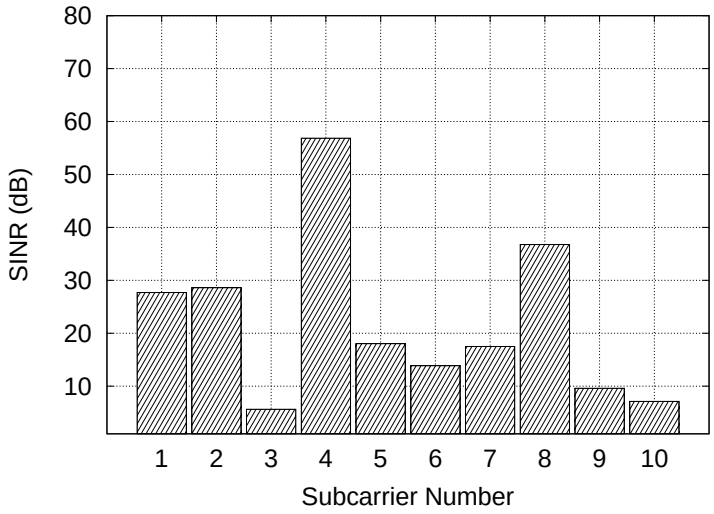

Figure 4.4: SINR distribution without IR

Figure 4.4 shows the distribution of SINR for MAS. The SINR value for fixed 10 sensor RF tags with MAS is analyzed. The analysis reveals that the interfered subcarrier has low SINR and because of that the average communication capacity is less for that particular subcarrier. The SINR value at subcarrier 4 and 8 is high because subcarrier 4 and 8 does not receive any harmonic from other subcarriers.

In Figure 4.5, the average communication capacity of 50 sensor RF tags with the same simulation behavior is compared with different allocation schemes when the harmonic rejection method is applied. When both the IR and allocation schemes are applied, the performance

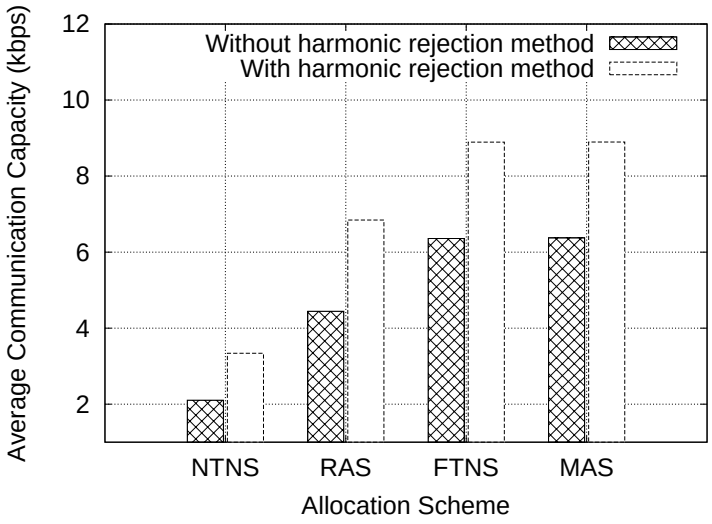

Figure 4.5: Average communication capacity comparison of 50 sensor RF tags

can be improved by 50% as compared to RAS without harmonic rejection. As the nearest sensor RF tag which has good SINR compared to the other sensor RF tags, assigned to nearest subcarrier generates more harmonic components which interfere to other subcarriers. Because of that, the average communication capacity decreases in NTNS. Our analysis shows that in all allocation schemes average communication capacity increase by approximately 30 to 35 % when harmonic rejection method is applied.

Figure 4.6 shows the fairness among 50 sensor RF tags. The Jain fairness Index [40] which is an indication of the user fairness of scheduling, provided by the different allocation schemes is employed.

To verify the simulation accuracy, the simulation run with a simple scenario in which all the sensor RF tags are uniformly distributed in the circle of radius R meter in random fashion with the same simulation setup in Table 4.1. The average communication capacity is calculated by simulation and numerical analysis. For simplicity, it is assumed there is no interference harmonic components generated from one subcarrier to other subcarrier, $i.e.$ there is no interference among the subcarriers.

The average communication capacity is calculated numerically using Eq. 4.5, where σ

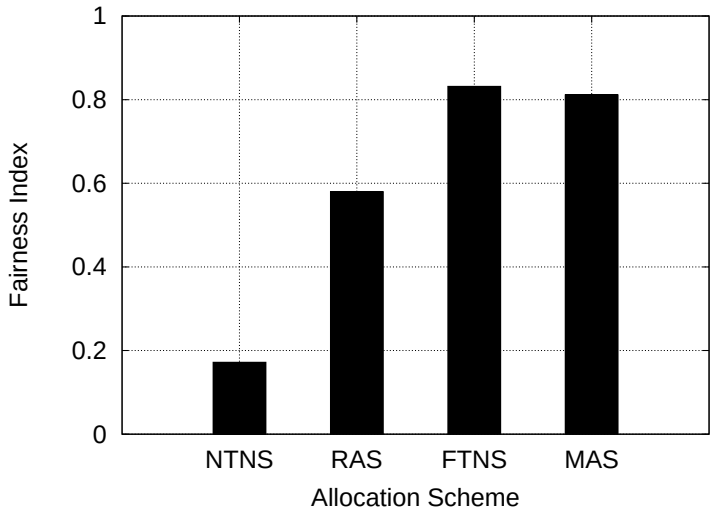

Figure 4.6: Fairness comparison

denotes the density of sensor RF tags in the circular area. C_n is communication capacity calculated numerically.

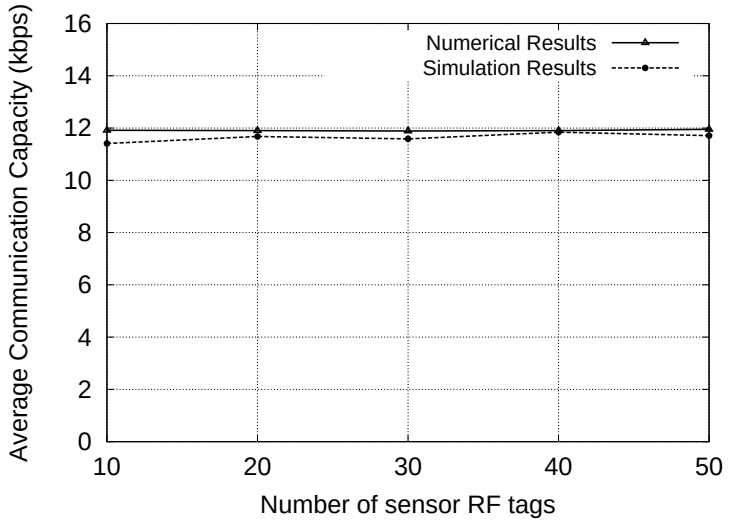

Figure 4.7: Average capacity comparison of numerical and simulation results

$$C_n = \frac{B \int_0^R 2\pi r\sigma \cdot \log_2 (1 + SINR) \cdot dr}{\int_0^R 2\pi r\sigma \cdot dr} \tag{4.5}$$

Figure 4.7 shows the average communication capacity calculated numerically and by simulation. It is found the average communication capacity is almost constant and nearly matches to the numerical result.

4.3 Variable Bandwidth Subcarrier Allocation

4.3.1 Introduction

In the previous Section 4.2 the channel allocation problem has been discussed in MSMA, where all the sensor RF tags demand an equal subcarrier bandwidth. Four allocation schemes are examined to reveal that allocating low subcarriers (low denotes the subcarrier is closed to the powering carrier frequency) to the geographically remote sensor RF tags and high subcarriers (subcarriers whose frequency is relatively far from the carrier frequency) to the geographically close sensor RF tags is, in general, advantageous in terms of the total communication capacity and fairness [40].

In this section, the channel allocation is extended to variable subcarrier bandwidth in MSMA. An exemplary variable bandwidth MSMA is where some sensor RF tags send only one axis acceleration measurement while others send three axes measurements. Later, the indecision cases where the two priorities on bandwidth and distance contradict are shown. A single performance index, total contamination power, is introduced to prioritize such indecision cases. The performance of the proposed scheme is evaluated with existing schemes in terms of the average communication capacity and system fairness using MATLAB.

4.3.2 Problem Statement and Evaluation Model

Let there be N sensor RF tags, each indexed as T_i ($i = 1 \ldots N$), located at distance r_i from the Reader/Writer. i-th sensor RF tag requires bandwidth b_i Hz at the subcarrier frequency f_i Hz. Let us assume that the available bandwidth, B Hz, is equal to the sum of the band-

width $B = \sum_{i=1}^{N} b_i$. To denote the variable bandwidth, the total bandwidth B is sub-divided into unit channels. This way, an arbitrary bandwidth can be represented as an aggregation of unit channels called subcarrier. The received signal power (S_i) of i-th subcarrier at the Reader/Writer depends on the distance r_i of sensor RF tag from the Reader/Writer. Since the free space loss as propagation model is used, the received signal power is proportional to $1/r_i^4$ of the transmitted power.

In MSMA, a subcarrier inevitably produces harmonics on odd multiples of primal subcarrier frequency. A subcarrier $(f_i \pm b_i/2)$ generates harmonics to other subcarrier bands as in Eq.4.6 with signal power (S_i/n^2) and thereby creates harmonic noise to the sensor RF tags operating at those frequencies.

$$nf_i \pm \frac{b_i}{2}, n = 3, 5, 7, \cdots \tag{4.6}$$

The harmonic noise h_{ij} created on f_j from other subcarriers f_i can be calculated as shown in Eq.4.7. Therefore, the total interference, H_j on a subcarrier f_j is obtained by adding the all harmonic noise on it as in Eq.4.10. It is clear that only a limited group of subcarrier frequencies f_i ($i \leq \frac{j}{3}$) incur harmonics on f_j.

$$h_{ij} = \begin{cases} \frac{S_i}{n^2} & \text{if}(\frac{j}{i} = n = 3, 5, 7 \cdots) \\ 0 & else \end{cases} \tag{4.7}$$

$$H_j = \sum_{i=1}^{\lfloor j/3 \rfloor} h_{ij} \tag{4.8}$$

The communication capacity E_i of sensor RF tag i is quantified with Shannon formula (Eq.4.9). The total system capacity of all sensor RF tags is obtained by simply adding them as in Eq.4.10

where n_T denotes the constant thermal noise coefficient.

$$E_i = \sum_{i=1}^{N} b_i \log_2(1 + SINR_i) \tag{4.9}$$

$$E = \sum_{i=1}^{N} E_i = \sum_{i=1}^{N} b_i \log_2(1 + \frac{S_i}{H_i + n_T b_i}) \tag{4.10}$$

The problem is to divide B Hz into N subcarrier bands ($f_i \pm b_i/2$) and allocate to N sensor RF tags such that the total communication capacity E is maximized. An example of channel allocation is shown in Fig.4.8.

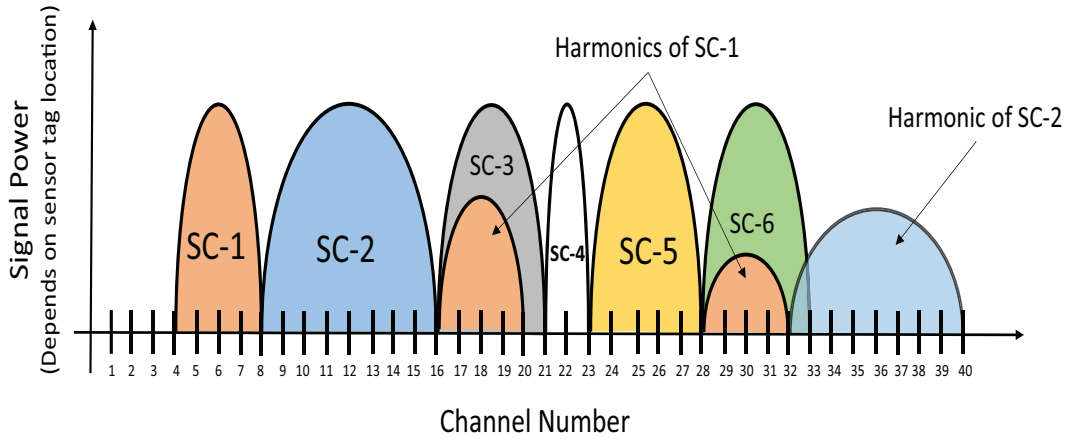

Figure 4.8: Harmonics interfere to other subcarriers, when subcarrier bandwidth is variable

It should be noted that some of the interference may spread over more than one unit channel as shown in Fig.4.8.

4.3.3 Channel Allocation Scheme

Section 4.2 reveals that the allocating low frequencies to remote sensor RF tags principle works for a constant subcarrier bandwidth MSMA system. It is denoted as FT (Far Tags to low frequency) scheme. A straightforward extension of the principle which prioritizes less interfering subcarriers to low frequencies to the variable bandwidth MSMA is to allocate

low frequencies to wide bandwidth subcarriers. It denote as WB (Wide Bandwidth to low frequency) scheme. The reverse priority is also examined, which is to allocate low frequencies to narrow bandwidth subcarriers. It is referred to as NB (Narrow Band to low frequency) scheme expecting NB is inferior to WB.

Figure 4.9 shows a comparison of NB and WB schemes when three sensor RF tags are located at the same distance. It is shown that the harmonics produced by narrow bandwidth sensor RF tags (T_1) fall in the available bandwidth when narrow bandwidth sensor RF tag is prioritized (allocated first). On the other hand, when the wide bandwidth sensor RF tag (T_3) is prioritized there is no harmonics in the available bandwidth. The reason of NB's inferiority to WB is the wide spread of harmonics in the available bandwidth.

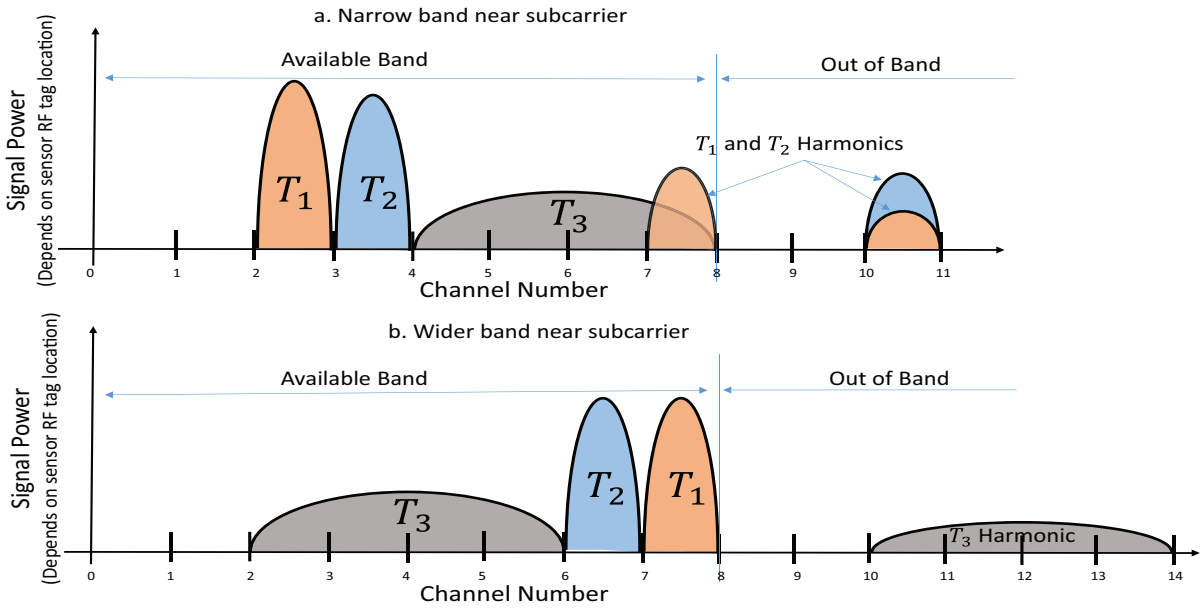

Figure 4.9: An example to compare NB and WB allocation schemes

This comparison of NB and WB provides an insight of general performance index. Apparently, the indecision case is when allocation schemes try to prioritize either a wide bandwidth sensor RF tag close to the Reader/Writer or a narrow bandwidth sensor RF tags located remote from the Reader/Writer. As a simple index to prioritize such indecision cases, an index

referred to as total contamination power (CP), is invented. CP is the summation of power of both principal subcarrier and harmonics in the available bandwidth as shown in Fig.4.10.

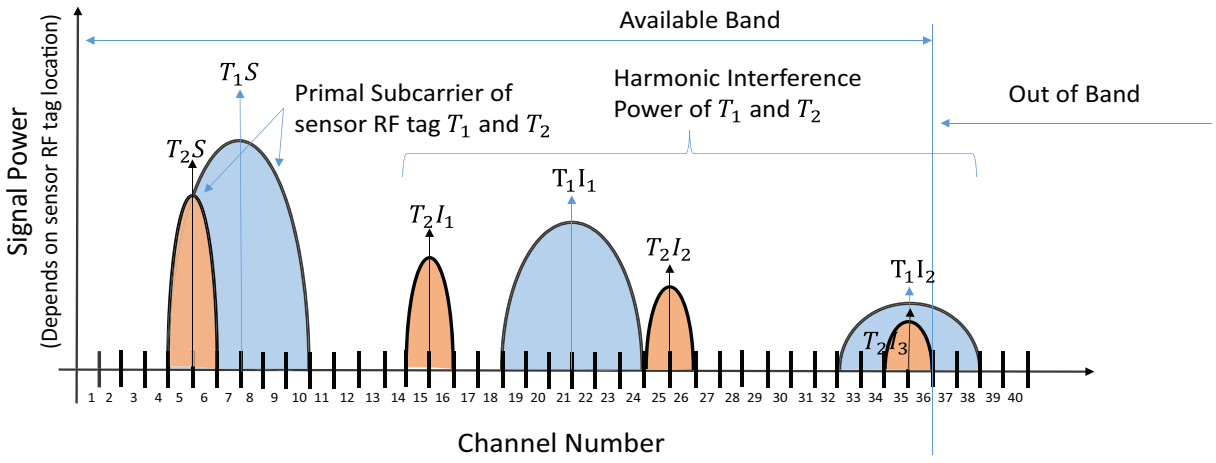

$\mathrm{CP_{T1}} = T_1S + \mathrm{T_1I_1} + \mathrm{T_1I_2}/3$

$\mathrm{CP_{T2}} = T_2S + \mathrm{T_2I_1} + \mathrm{T_2I_2} + \mathrm{T_2I_3}$

T_iS: Primal Subcarrier Power of $\mathrm{T_i}$

$\mathrm{T_iI_j}$: $\mathrm{j^{th}}$ Harmonic Interference Power of $\mathrm{T_i}$

$\mathrm{CP_{Ti}}$: Contamination Power of $\mathrm{T_i}$

Figure 4.10: Total contamination power for sensor RF tag T_1 and T_2 located at different distance

CP scheme basically tries to reduce the total power into the available bandwidth. Prioritizing the small contamination power sensor RF tags to low frequencies, regardless of distance and the bandwidth is expected to minimize the interference and consequently results in a good communication capacity.

The pseudo codes of the four schemes are listed in Algorithms 5-8.

Algorithm 5 FT: Far Tag to low subcarrier

T is a list of sensor RF tags, arranged in decreasing order based on their distance.
C is the total number of channels. Initialize i = 1 and j = 0;
c is required channel by a sensor RF tag T_i;
while $j \leq \lceil C/3 \rceil$ **do**
    Pick the sensor RF tag T_i from the list.
    Allocate required c unit channels from j to $j + c$ to T_i, delete T_i from the list.
    $i \leftarrow i + 1$; $j \leftarrow j + c$;
end while
Arrange the list T in reverse order.
Pick a sensor RF tag from the list, allocate its require unit channels and continue this step.

Algorithm 6 NB: Narrow Bandwidth to low subcarriers

T is a list of sensor RF tags, arranged in increasing order based on their required channel badnwidth.
C is the total number of channels. Initialize i = 1 and j = 0;
c is required channel by a sensor RF tag T_i;
while $j \leq \lceil C/3 \rceil$ **do**
    Pick the sensor RF tag T_i from the list.
    Allocate required c unit channels from j to $j + c$ to T_i, delete T_i from the list.
    $i \leftarrow i + 1$; $j \leftarrow j + c$;
end while
Arrange the list T in increasing order based on sensor RF tag location.
Pick a sensor RF tag from the list, allocate its require unit channels and continue this step.

Algorithm 7 WB: Wide Bandwidth to low subcarriers

T is a list of sensor RF tags, arranged in decreasing order based on their required channel badnwidth.
C is the total number of channels. Initialize i = 1 and j = 0;
c is required channel by a sensor RF tag T_i;
while $j \leq \lceil C/3 \rceil$ **do**
    Pick the sensor RF tag T_i from the list.
    Allocate required c unit channels from j to $j + c$ to T_i, delete T_i from the list.
    $i \leftarrow i + 1$; $j \leftarrow j + c$;
end while
Arrange the list T in increasing order based on sensor RF tag location.
Pick a sensor RF tag from the list, allocate its require unit channels and continue this step.

Algorithm 8 CP: low Contamination Power to low subcarriers

1: T is a list of all sensor RF tags.
2: C is the total number of unit channels.
3: c is required channel by a sensor RF tag T_i;
4: U is the used channels.
5: Initialize U=0 and i = 1.
6: **while** $U \leq \lceil C/3 \rceil$ **do**
7: **for** $j = 1 : N + 1 - i$ **do**
8: Calculate contamination power for the sensor RF tag T_j.
9: **end for**
10: Find the sensor RF tag t has minimum contamination power, calculated in last step.
11: Assign the sensor RF tag t to its require channels, say, c. Delete the sensor RF tag t from the list T.
12: $i \leftarrow i + 1$; $U \leftarrow U + c$
13: **end while**
14: Arrange the list T in increasing order based on sensor RF tag location.
15: Pick a sensor RF tag from the list, allocate its require unit channels and continue this step.

4.3.4 Evaluation

A Monte Carlo simulator is developed with MATLAB to evaluate the proposal and the counter schemes. In one round of Monte Carlo simulation, N sensor RF tags are randomly distributed in a circular region of radius 10 meter where the Reader/Writer is always located at the center. The minimum distance between the Reader/Writer and the sensor RF tag is set to be 1 meter. Table 4.2 shows the details of simulation parameters.

The four schemes, FT, WB, NB and CP, are applied in each round, if applicable, and the total communication capacity divided by the number of sensor RF tags and the channel allocation are recorded. After the completion of predefined number of simulation rounds, the average communication capacity of the four schemes are derived. The pseudo code of X times Monte Carlo simulation is shown in Algorithm 9.

Algorithm 9 Simulation Method

```
X is number of simulation runs, X = 100.
Y is different allocation schemes.
N is number of sensor RF tags
for i = 1 : X do
    Random and uniform distribution of N sensor RF tags in the circular region
    for j = 1 : Y do
        Allocate subcarrier channels according to scheme
        Evaluate signal power and harmonic noise power on each sensor
        Evaluate signal to noise ratio (SINR), average communication capacity, fairness index
    end for
end for
Generate average performance parameters for each allocation scheme
```

To denote a set of variable bandwidth, "Class" is introduced which denotes the number of required unit channels and "Scenario" which denotes the distribution of sensor RF tags in each Class. The four Classes and two Scenarios are used as in Table 4.3 such that each Scenario provides the same available bandwidth. A general formula to calculate available bandwidth in particular Scenario is, C1 sensor RF tags $\times$ 1 + C2 sensor RF tags $\times$ 2 + C3 sensor RF tags $\times$ 3 + C4 sensor RF tags $\times$ 4. (For example, if there is eight sensor RF tags in Scenario 1, total available channels = 2 $\times$ 1 + 2 $\times$ 2 + 2 $\times$ 3 + 2 $\times$ 4 = 20 channels. To provide the same bandwidth in Scenario 2, ten sensor RF tag are considered, total available channels = 4 $\times$ 1 + 3 $\times$ 2 + 2 $\times$ 3 + 1 $\times$ 4 = 20 channels.)

To show the advantage of CP scheme, the following three different simulation cases are evaluated.

1. The first case is where all the sensor RF tags demand an equal bandwidth. In this case, only CP and FT are used. CP shall provide the equivalent allocation and performance to FT.

2. The second case is where all the sensor RF tags are located at the same distance and demand different bandwidth subjected to Scenario 1. In this case CP scheme shall provide the same allocation and performance to WB.

3. The third case is where sensor RF tags demand variable bandwidth based on a Scenario and their distances from the Reader/Writer are randomly chosen.

Table 4.2: Simulation setup parameter

Simulator	MATLAB
Unit channel bandwidth	1 KHz
Network layout	Single-cell with omni-direction antenna
Total # of Subcarrier	Equal to # of sensor RF tag
Reader/Writer antenna gain	0dBi
Reader/Writer transmitting power	1W
Sensor RF tag position	Stationary

Finally, the accuracy of simulation is verified by comparing results with the brute force method for eight sensor RF tags. For more than eight sensor RF tags, the brute force method computation becomes infeasible even with a high-performance workstation (HP Workstation Z230 - Xeon E3-1245V3 3.4 GHz) because of significant number of permutations.

Table 4.3: Distribuition of sensor RF tags in four classes

Class Number	Rq. # of channels	Scenario-1	Scenario-2
C1	1	25%	40%
C2	2	25%	30%
C3	3	25%	20%
C4	4	25%	10%

4.3.4.1 Case-1: sensor RF tags require equal bandwidth subcarrier located at varying distance

Figure 4.11 shows the comparison of average communication capacity with FT and CP schemes, when all sensor RF tags require an equal bandwidth. All sensor RF tags are considered to be in Class C1. It can be seen that both CP and FT shows similar performance. The average communication capacity of both schemes decrease as the number of sensor RF tag increases.

This is because the number of harmonics in the available bandwidth increases as the number of sensor RF tags increases.

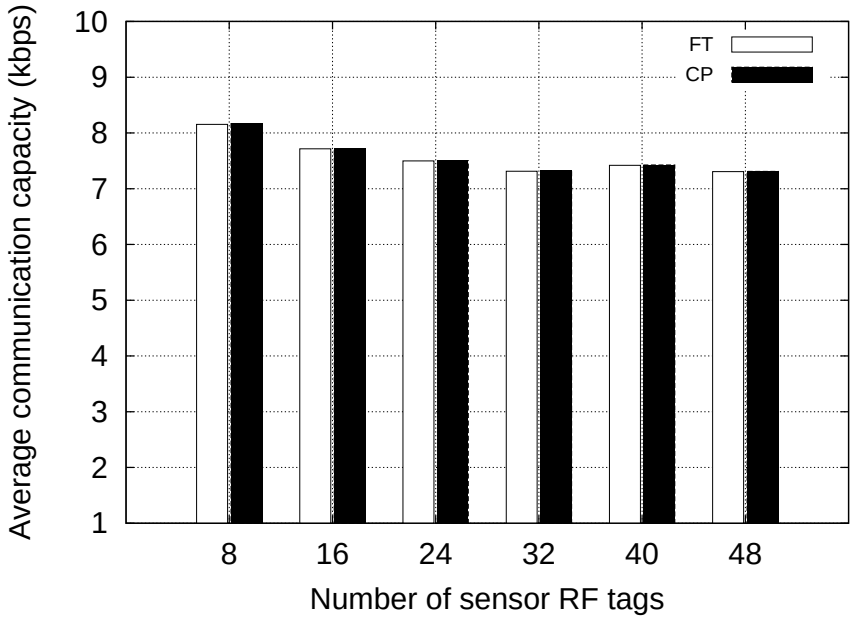

Figure 4.11: Comparison of average communication capacity for FT and CP schemes when all sensor RF tags require unit bandwidth channel in Scenario-1

4.3.4.2 Case-2: sensor RF tags located at same distance require varying bandwidth subcarrier

All four allocation schemes are evaluated in this case and the results are shown in Fig.4.12. The fixed distance of the sensor RF tags is chosen to be 6 m. It can be seen that CP scheme performs the best and equivalently to WB. FT does not perform well because FT cannot prioritize the bandwidth. NB shows the worst performance as predicted.

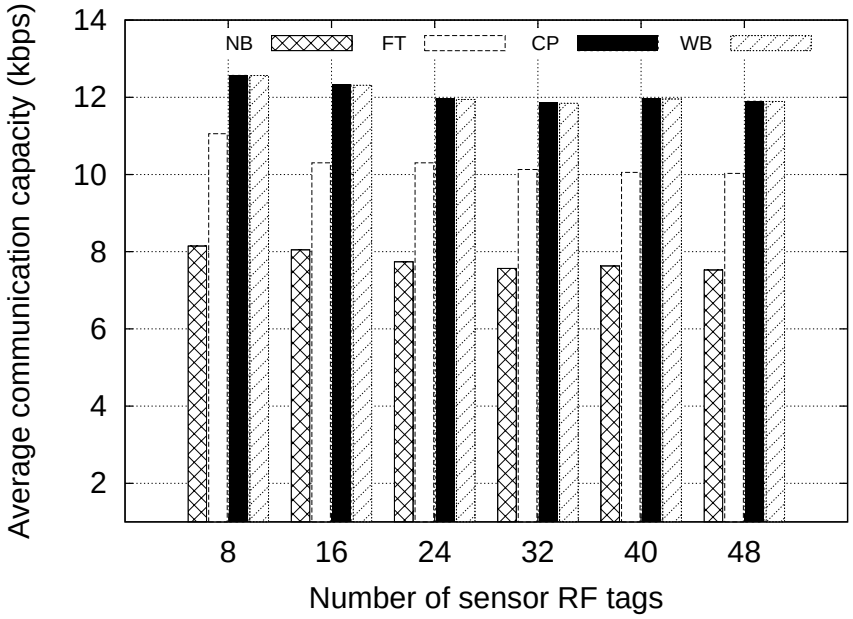

Figure 4.12: Comparison of average communication capacity when all sensor RF tags are located at equal distance (6 meter) in Scenario-1

4.3.4.3 Case-3: sensor RF tags located at varying distance require varying bandwidth subcarrier

The average communication capacity with the four schemes subjected to Scenarios 1 is shown in Fig.4.13. It is shown CP outperforms other schemes. FT performs closely to CP while WB contributes little. The difference of FT and WB performance can be explained such that the difference of distance spans from 1m to 10m which results in 10000 times difference with the free space loss assumption while the difference of bandwidth is four at most. NB performs worst in this case too. The robustness of CP is confirmed in Scenario 2 as shown in Fig.4.14.

For this particular case, the system fairness for Scenario 1 is evaluated. Figure 4.15 shows the fairness of the four schemes. FT and CP are equivalent and the best performance. The achieved fairness 0.8, which is not necessarily good, stems from the wide variation in sensor RF tags location (far and close to the Reader/Writer) compare with their require bandwidth.

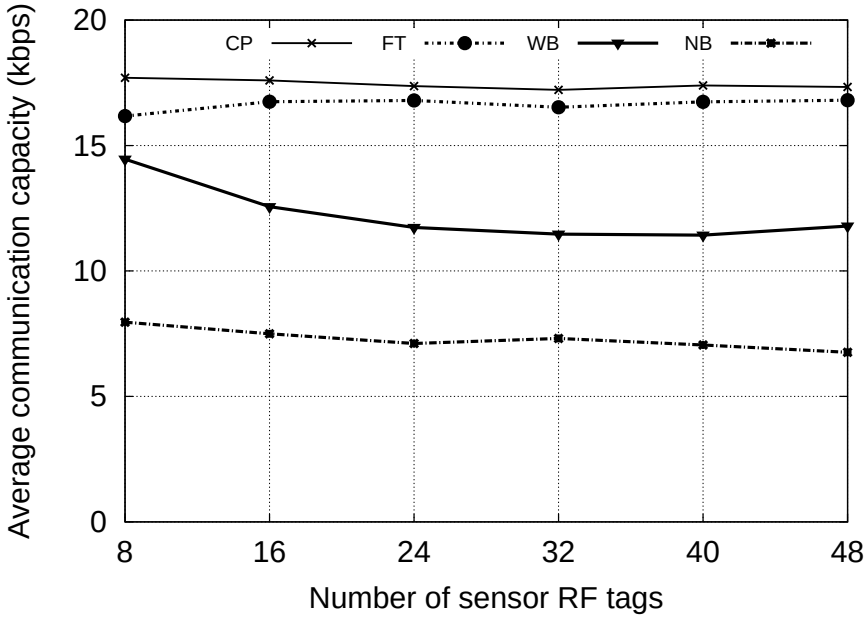

Figure 4.13: Comparison of average communication capacity for different allocation scheme in Scenario 1

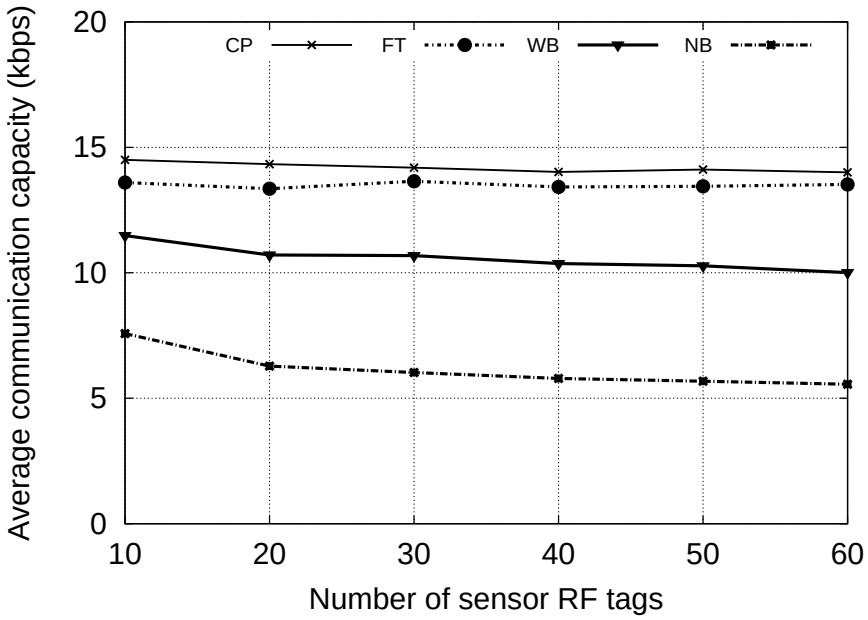

Figure 4.14: Comparison of average communication capacity for different allocation scheme in Scenario 2

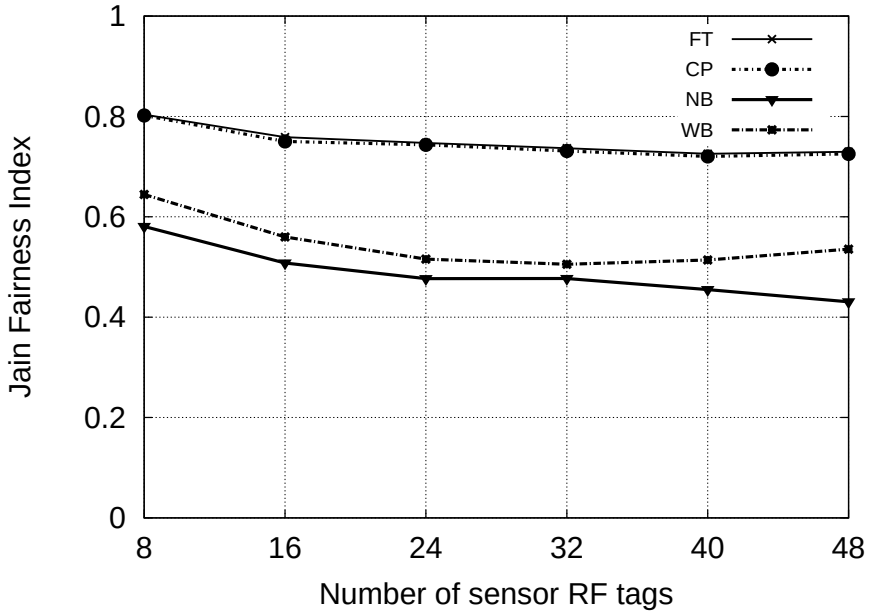

Figure 4.15: Comparison of fairness index for different allocation scheme

4.3.4.4 Analysis of CP scheme for Other Cases

This section additionally reports the performance of CP scheme when the assumptions in the channel allocation are modified in two ways. Firstly, it introduces service grade to prioritize the channel allocation. It shows that the high service grade sensors could be allocated to good quality channels simply by introducing a service grade coefficient in CP scheme. Secondly, it examines the case where the number of available channels are larger than the total sum of the sensors bandwidth. Later, the scheme shows that the spare frequency channels can be effectively used to increase the total performance.

When the sensor RF tags have different service grade (SG)

In Section 5.2, FT, NB and WB schemes are examined considering the distance or bandwidth parameter in the subcarrier allocation. However, the different parameters may require in the subcarrier allocation. Therefore, the proposed algorithm CP scheme redefined by in-

Algorithm 10 Priority based CP scheme

1: T is a list of all sensor RF tags.
2: C is the total number of unit channels.
3: c is required channel by a sensor RF tag T_i;
4: U is the used channels.
5: Initialize $U = 0$ and $i = 1$.
6: **while** $U \leq \lceil C/3 \rceil$ **do**
7: **for** $j = 1 : N + 1 - i$ **do**
8: Calculate contamination power for the sensor RF tag T_j.
9: multiply contamination power with α. Hence, $CP_j = CP_j * \alpha$
10: **end for**
11: Find the sensor RF tag t has minimum contamination power ($min.(CP_j)$), calculated in last step.
12: Assign the sensor RF tag t to its require channels, say, c. Delete the sensor RF tag t from the list T.
13: $i \leftarrow i + 1; U \leftarrow U + c$
14: **end while**
15: Arrange the list T in increasing order based on sensor RF tag location.
16: Pick a sensor RF tag from the list, allocate its require unit channels and continue this step.

troducing a factor α defines the application SG, such that the pseudo code for generalized CP scheme is modified and shown in Algorithm 10, where α is a coefficient to define SG.

The simulation considers the two different SG of sensor RF tags, low-SG, and high-SG. The α sets to 1 and 3 for the high-SG and low-SG sensor RF tags, respectively, $i.e$, the low value of α for a sensor RF tag has the high-SG. The other simulation parameters are taken as same as in Section 4.2, whereas the low-SG and high-SG sensor RF tags are divided uniformly.

Figure 4.16 shows the average communication capacity of CP scheme when the sensor RF tags are divided into low-SG and high-SG. It is shown that the CP scheme before considering the SG parameter gives an almost equal performance for both low-SG and high-SG sensor RF tags. However, when considering the priority factor the communication capacity for high-SG sensor RF tags is increased because the scheme gives priority to high-SG sensor RF tags in channel allocation.

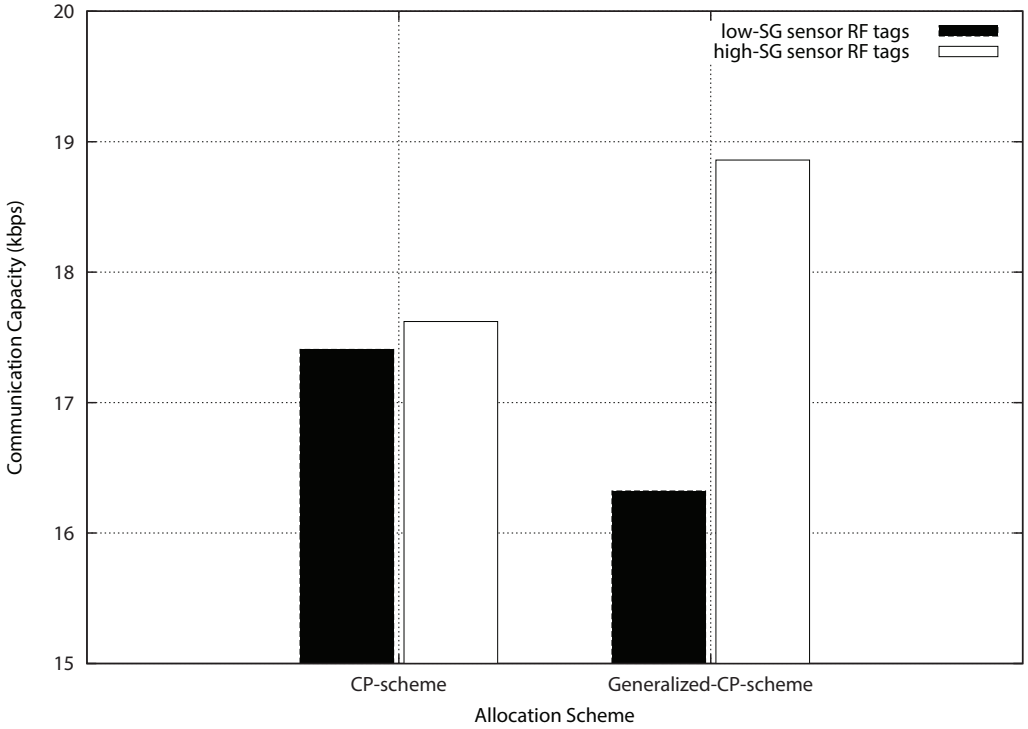

Figure 4.16: Average communication capacity with CP scheme when sensor RF tags have different SG.

When available bandwidth is more than the required bandwidth

When the number of available channels is larger than the required channels, the scheme saves the extra channels from near end and start allocation afterward. By doing that the interference can be decreased in the remaining channels. Figure 4.17 shows the average communication capacity of CP scheme when the number of available channels increases while a number of sensor RF tags are fixed to eight. The other simulation parameters are the same as in Table 4.2. In the simulation, the sensor RF tags location are fixed while increasing the number of available channels. It is shown that the communication capacity increases as the number of channel increases and later it saturates. It is because when the allocation starts after the one-third of available channels, there is no interference.

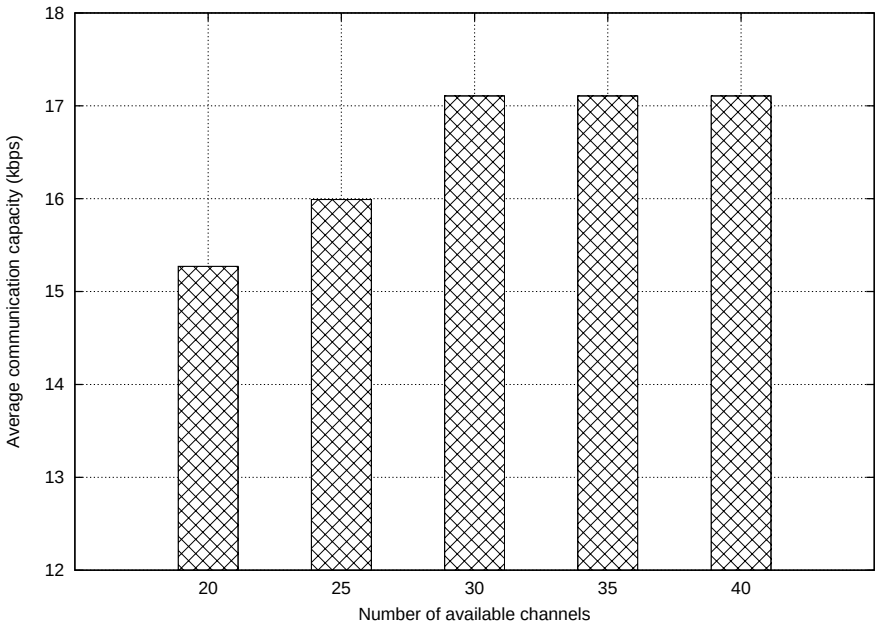

Figure 4.17: Average communication capacity with CP scheme when the number of sensor RF tags is constant and the number of available channels increases.

4.3.4.5 Examination CP Scheme with Brute Force Method

For the verification purpose, CP scheme is compared with the brute force method with eight sensor RF tags under Scenario 1. As in the other simulation cases, 100 times Monte Carlo simulation is carried out. In the brute force method, the simulation examines all the permutations and extracts the allocation which gives the best average communication capacity. The total number of combinations examine is, therefore, $40320 = 8!$ for eight sensor RF tags.

Figure 4.18 shows the average communication capacity of CP scheme and the brute force method. It is shown CP performs equivalently to the brute force method. To understand the difference, the allocation outcomes are compared as in Table 4.4 and also the allocation pattern is shown pictorially in Fig.4.20. CP and the brute force method both prioritize sensor RF tag T_5 over sensor RF tag T_2 where the two sensor RF tags are in indecision combination — sensor RF tag T_5 demands a wider bandwidth whereas it is relatively near the Reader/Writer compared to sensor RF tag T_2. Two schemes choose differently for the third subcarrier. This is also an

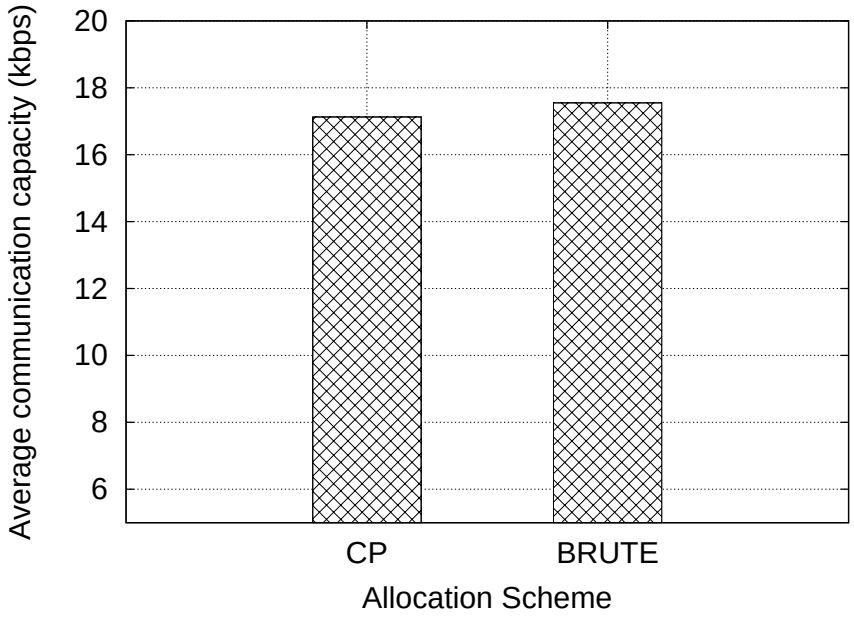

Figure 4.18: Comparison of average communication capacity of CP scheme and brute force for eight sensor RF tags

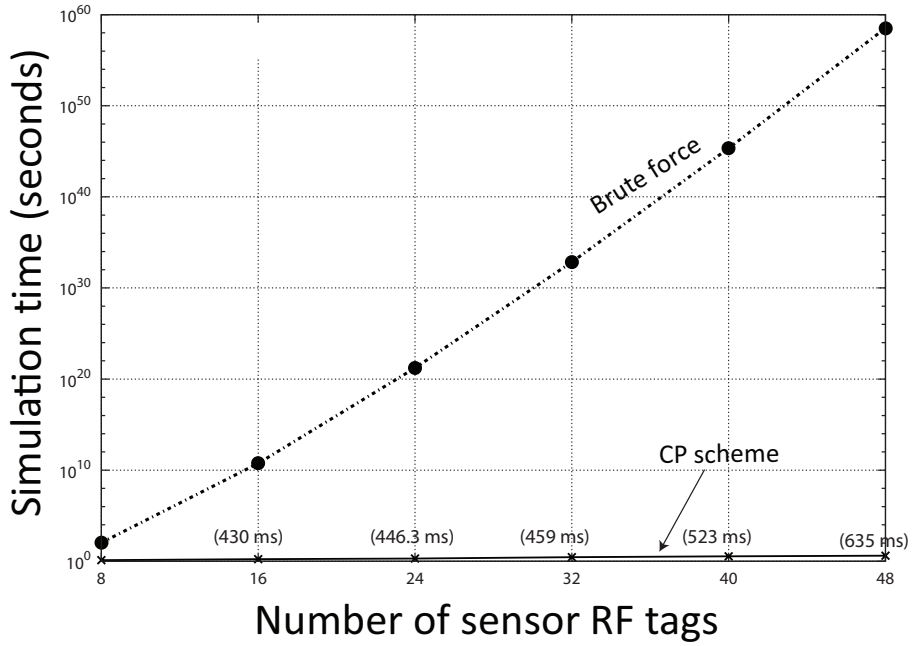

Figure 4.19: Comparison of simulation execution time for CP scheme and brute force calculated theoretically

indecision case of sensor RF tags T_6 and T_7. CP chooses T_6 instead of T_7 because either choice does not generate harmonic in the available bandwidth. In terms of the contamination power, therefore, the remote sensor RF tag has priority. The choice does not entail a big difference in the communication capacity.

Sensor RF tag	T_1	T_2	T_3	T_4	T_5	T_6	T_7	T_8	-
Rq. channels	1	1	2	2	3	3	4	4	-
Located at	2.6	9.5	4.7	5.0	8.7	6.3	5.1	3.1	-
Subcarrier #	1	2	3	4	5	6	7	8	capacity
CP	T_5	T_2	T_6	T_1	T_8	T_3	T_4	T_7	16.01
Brute	T_5	T_2	T_7	T_1	T_6	T_3	T_8	T_4	16.45

Table 4.4: An example to compare subcarrier allocation pattern for CP scheme and brute method

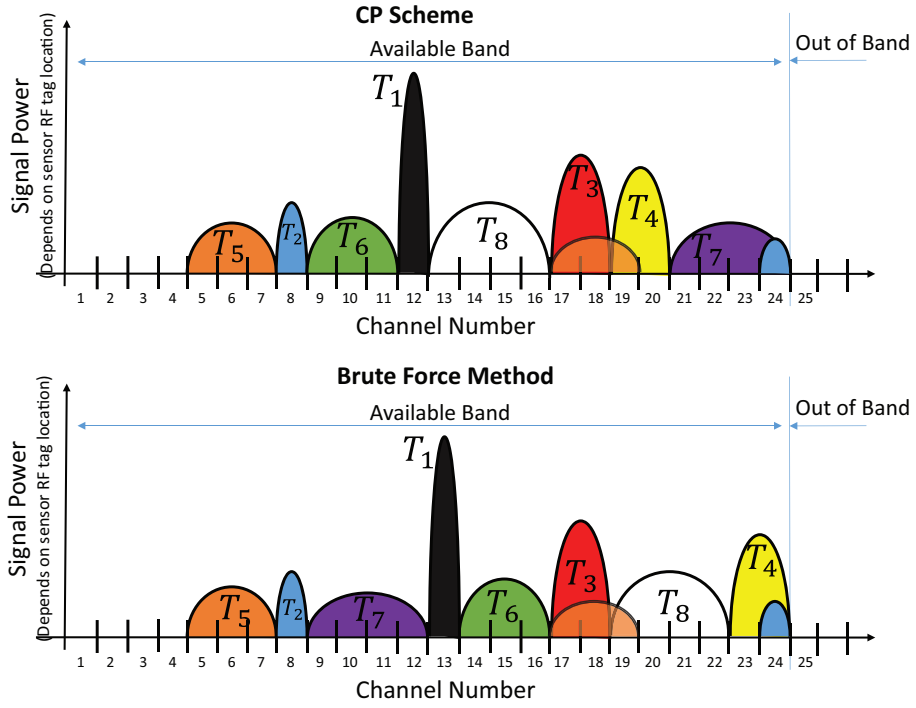

Figure 4.20: The pictorial representation of allocation pattern for CP scheme and brute method

CP scheme not only leads to sub-optimized performance, but also minimizes implemen-

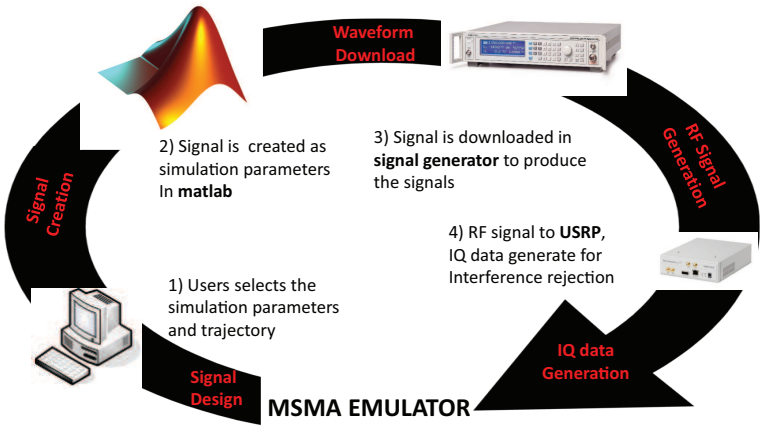

Figure 4.21: MSMA system evaluation can be performed without physically place the sensor tag by using MSMA emulator

tation complexity (execution time). Since achieving better optimality normally requires more complicated resource allocation algorithms, sub-optimal algorithms with lower complexity are of practical interests The time complexity of CP is $O(N^2)$ which makes it more practical and better compared with the other schemes. Figure 4.19 shows the comparison of simulation time calculated theoretically for brute force method and CP scheme. It can be seen that the execution time for CP scheme is far less than that the brute force method.

4.4 MSMA Emulator Development

When evaluating channel allocation method, placing large number of sensor RF tags physically is inefficient. Therefore MSMA signal emulator using MATLAB is developed and used in the evaluation.

Figure 4.21 shows the steps of emulator for generating sensor signals. First, the user configures simulation parameters such as a number of sensors, minimum and maximum distance from the Reader/Writer etc. After this step MATLAB creates the subcarrier signal based on the input parameters and further, the signal is downloaded into a signal generator which pro-

Signal Architect SW	
Operating System	Windows-7/8
Multi-core Support	HP Z230 workstation - Core i7 4790 3.6 GHz
Software	MATLAB 2015b
Signal Download HW	
Hardware	Signal Generator
Interface	Gigabit Ethernet (GbE)
SDR Control Unit	
RF in/out	SAM connector for input/output
RF record	Channel center frequency 916.8 MHz NI-USRP RIO Sample frequency 2-20 MHz
Future System Option	Multi-RF channel

Figure 4.22: Signal emulator system specification

duces radio frequency signal to USRP and the IQ data can be collected. Figure 4.22 shows the system parameter of MSMA emulator.

First, the emulator generates a square wave of particular subcarrier frequency after that the baseband signal is encoded with Miller encoding. Finally, the modulated subcarrier signal is generated by taking XOR of Miller encoded signal as shown in Fig.4.23 for 10KHz modulated subcarrier signal. To better understand the modulated subcarrier signal digital modulation is considered whereas the experiment is done with the sensor RF tag which modulates the sensor data with analog modulation techniques.

To verify the proposed allocation schemes Bit Error Rate (BER) is measured for different allocation schemes in fixed bandwidth subcarrier and variable bandwidth subcarrier, before applying the harmonic rejection method. The five sensor tags are assumed to be located at the different distance require different subcarrier bandwidth. The backscatter signal of all the sensor RF tags is generated with emulator environment. To visualize the effect of subcarrier assignment schemes the BER is measured before applying the harmonic rejection. A Lab-VIEW program is developed to measure the BER where ASK demodulation has been done on the baseband signal. The output stream is compared with the original bit stream.

Figure 4.24 shows the measured BER for different allocation scheme. The lower BER

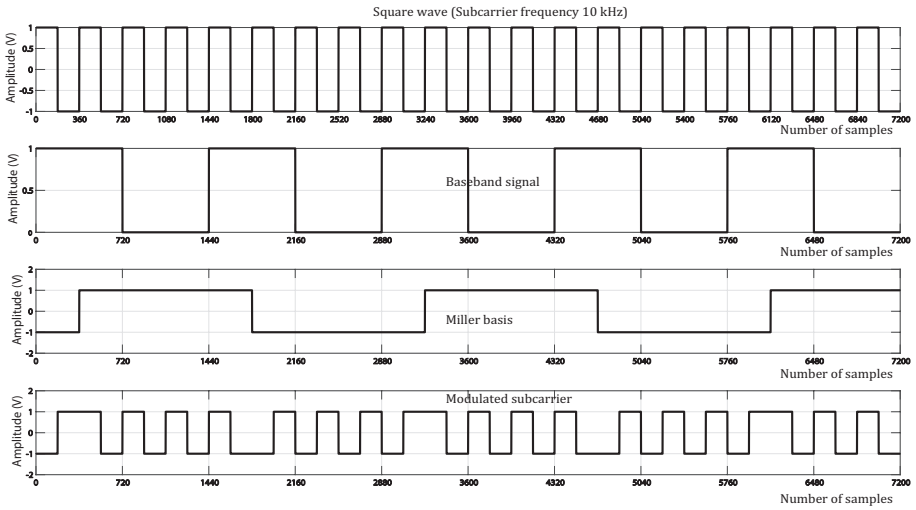

Figure 4.23: Miller encoded modulated subcarrier signal for a sensor tag

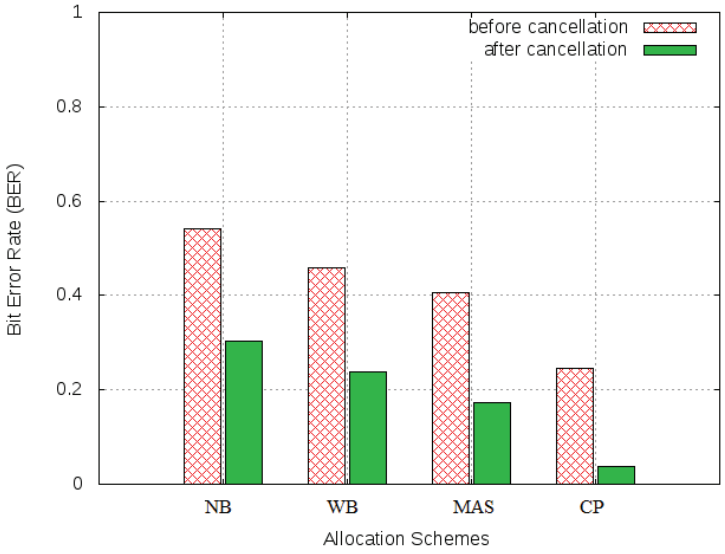

Figure 4.24: Measured BER before interference rejection method for different subcarrier allocation schemes in both cases fixed bandwidth subcarrier and variable bandwidth subcarrier.

means the better performance. It can be seen that CP schemes works better than other allocation schemes because it considers both distance and the required bandwidth in the channel allocation.

4.5 Summary

Even though the interference can theoretically be canceled by applying signal processing in the Reader/Writer, careless allocations of subcarrier frequency may lead to poor communication capacity and poor fairness. Since the subcarriers close to the powering carrier frequency influential to other subcarriers strongly influence other subcarriers, those subcarrier channels should be allocated to sensor RF tags that are furthest from the Reader/Writer. The simple allocation scheme achieves almost optimal performance, about 50% greater communication capacity than randomly chosen subcarrier allocation.

The challenge of subcarrier allocation in variable bandwidth MSMA is the arbitration among bandwidth and the distance of sensor RF tag. The general rule of thumb is to allocate one third of available bandwidth to remote or wide bandwidth sensor RF tags since the low frequencies entail more interference in the available bandwidth than the high frequencies. To prioritize either a wide bandwidth and remote sensor RF tag or a narrow bandwidth and close sensor RF tag, total contamination power index is introduced which can handle the two criteria simultaneously. By using the total contamination power index, the original permutation combinatorial problem $O(N!)$ can be simplified to $O(N^2)$ problem, thus significantly reducing the computation time. Yet the proposed method achieves almost equivalent performance in terms of communication capacity and fairness compared with the true optimized solution.

Chapter 5

MSMA Evaluation with Vibration Testing

5.1 Introduction

This chapter evaluates the performance of harmonic rejection method with a prototype of MSMA system in a vibration test setting. An experiment is configured to emulate a scenario where three sensor RF tags are mutually interfered. The performance and accuracy of MSMA system are compared with the attached commercial wired sensors vibration testing system.

5.2 Vibration Testing Setup

Figure 5.1 shows the vibration testing setup. A metal plate is fixed on the vibrator table. Wired sensor and wireless sensor RF tags are attached to the metal plate. The signal generator emulating a Reader/Writer keeps sending 916.8MHz CW at -10 dBm. The transmitted signal from the signal generator is amplified by 40dB to obtain 30dBm port power. The amplifier is connected to a transmitting antenna of 6dB. The experiment has been done with three sensor RF tags. The operating subcarrier frequency of sensor RF tags is chosen in such a way that the sensor RF tag 1 (10 kHz subcarrier frequency) interferes to the sensor RF tag 2 (30 kHz subcarrier frequency) and sensor RF tag 1 and 2 both interferes to the sensor RF tag 3 (90

kHz subcarrier frequency). The wired accelerometer sensor data acquisition is done by the multiplexer. The wireless sensor RF tags data is collected from the receiving antenna which is further connected to the splitter to analyze the signal on a spectrum analyzer. The signals are received by the software defined radio (SDR) device (NI USRP 2592R) which converts the received analog signal into IQ data.

Figure 5.2 shows pictures of experiment which has been done in the laboratory. The acceptable average phase error is less than about 10% of original amplitude yielding the criteria of less than 5 degree. The experiment has been done with the 50 Hz and 100 Hz exciting frequency with 1g acceleration limit. The frequency spectrum is measure by the RSA 507A USB Spectrum Analyzer for the received signal from all the sensor RF tags as shown in the Fig.5.3.

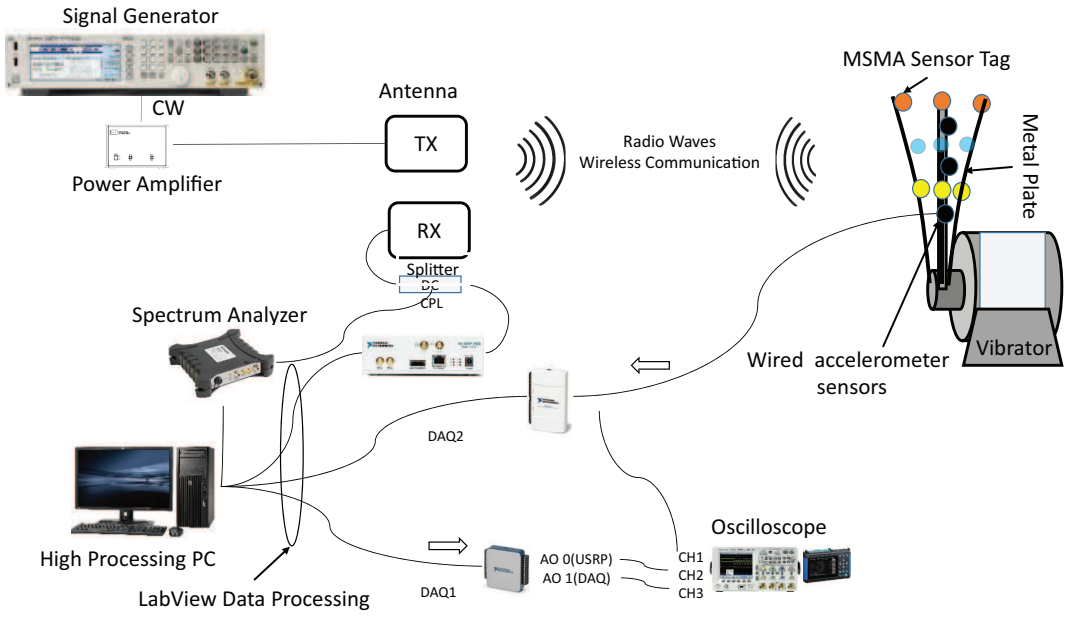

Figure 5.1: Vibration testing setup

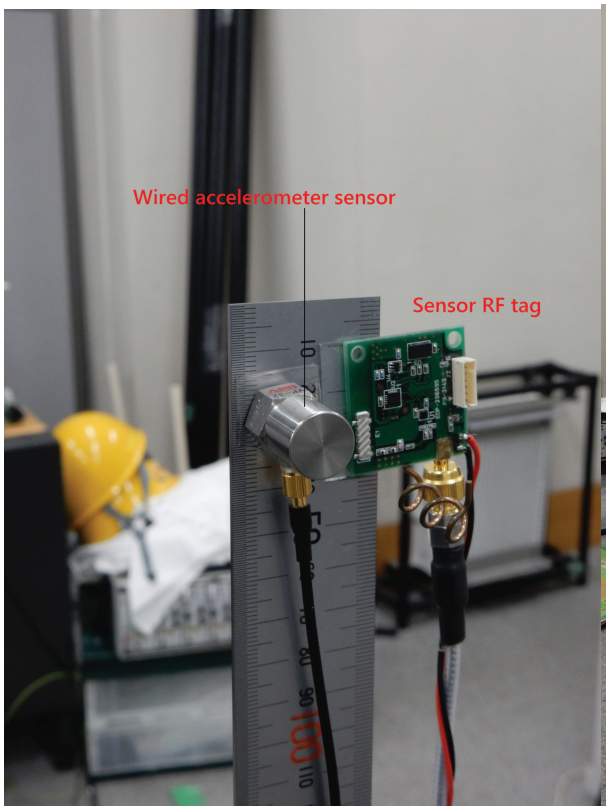

(a) Wired accelerometer sensors and sensor RF tags are attached nearly at the same position.

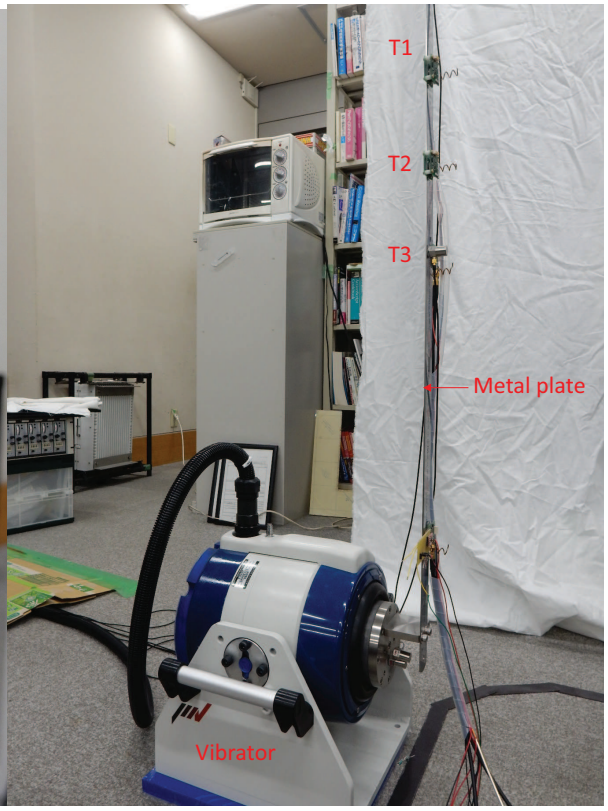

(b) Wireless sensor RF tags are attached to the metal beam.

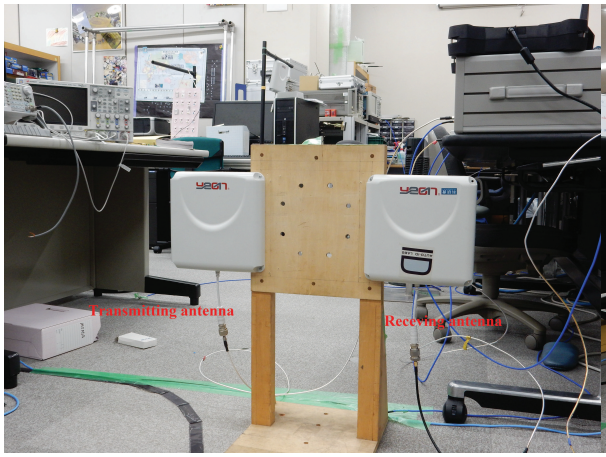

(c) Picture shows a transmitting and receiving antenna connect with a signal generator and USRP, respectively.

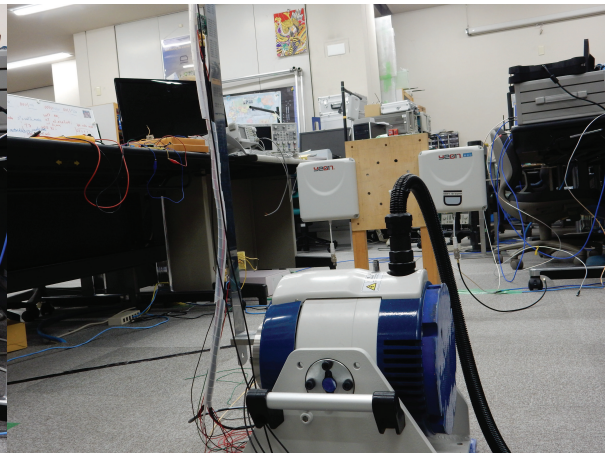

(d) Vibration test setting

Figure 5.2: Experimental vibration test setting in the laboratory.

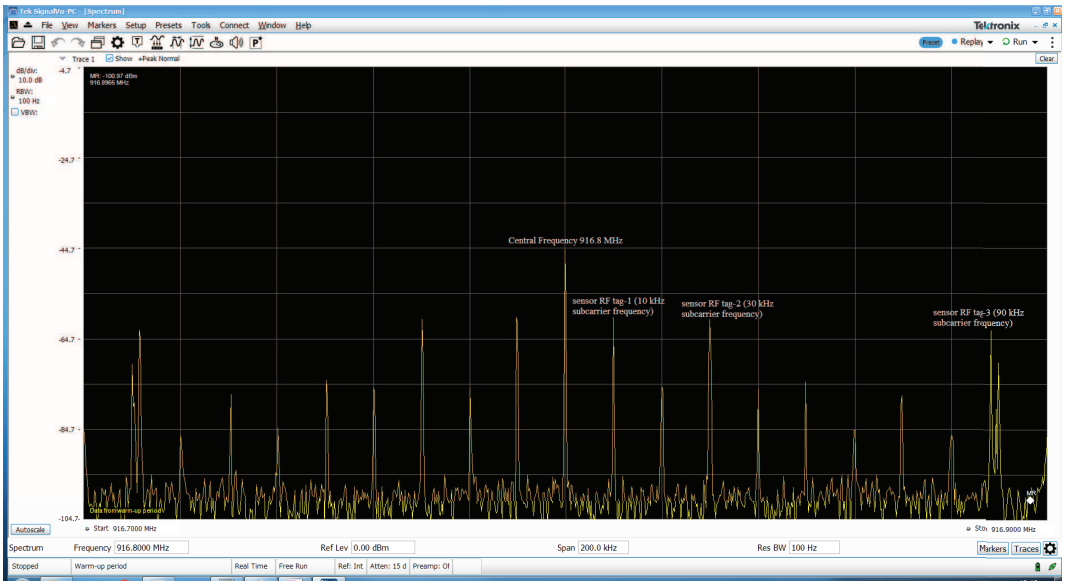

Figure 5.3: Frequency spectrum of the received signal from all three sensor RF tags.

5.3 Results and Analysis

Since the backscatter signal power is very small compared with the power of CW, the removal of the DC component is important to increase the resolution. On the other hand, the phase linearity of the process such as DC component removal is important. In Chapter 3, it is found that, in the case of multi-path free propagation environment (wired connection by SMA cable, etc.) that highly accurate replica can be generated by MSMA.

Previously at the software defined receiver side, all of the processing is done with the host PC (HP Z230 Xeon 3.4GHz 16GB Win7 64bit). In this experiment, FPGA is also used to process the data. Also the processing platform LabVIEW2016 is replaced by LabVIEW Communication 2.0 to improve the processing delay at SDR and to synchronize time for input (excitation signal) and output (observation signal) such as frequency response analysis. Accordingly, the reception processing time/real time ratio becomes significantly faster by a factor of 20.

The moving average filter with thousand taps works perfect when using an internal RC

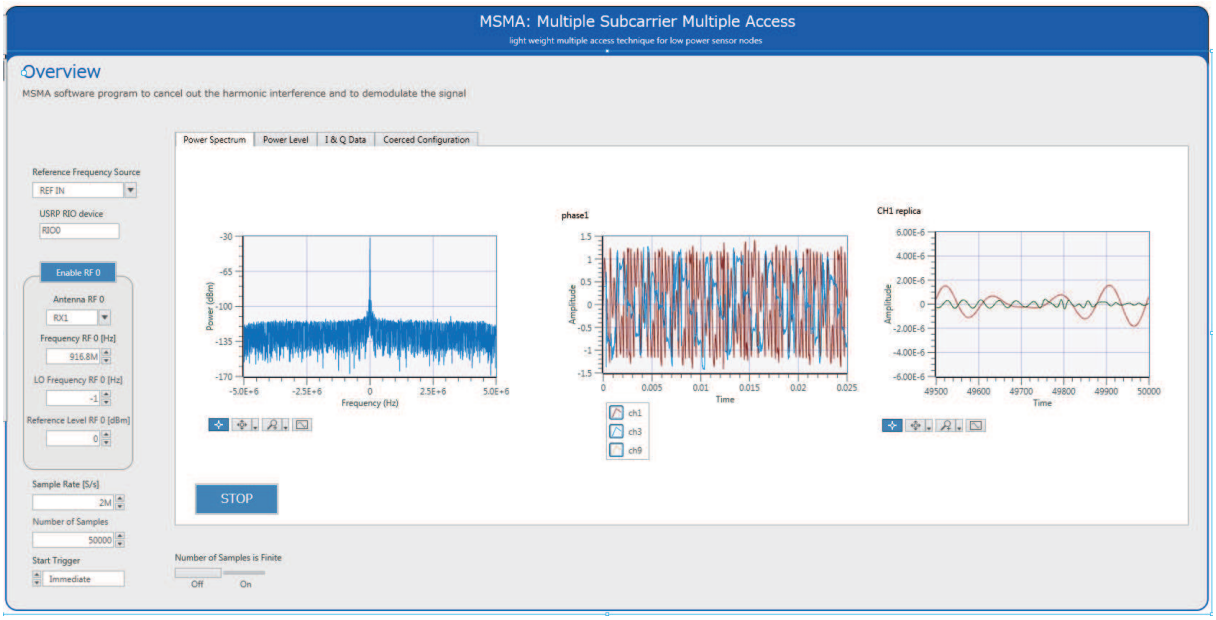

Figure 5.4: MSMA user interface in LabView Communication 2.0

resonator, the harmonic components can be canceled out 99% at 40dB. However there is a problem of processing delay with the moving average filter of several thousand taps. With the Infinite Impulse Response (IIR) filter known as DC blocker, the computational speed can be enhanced whereas the harmonic component removing effect is impaired but remains on the degree 99% at 20 dB in wired configuration. However, in the real propagation environment (measurement carried out indoors), the effect of the moving average filter becomes leveled off. The interference removal effect using either filter is above 14dB. It was found that sometimes performance becomes low (96% of the interference removal performance).

Figure 5.6 shows the signal received by wireless sensor RF tags before and after applying harmonic rejection method. It can be seen the data for channel 3 and channel 9 can be recovered after harmonic rejection method. However it still has some noise.

Figure 5.7a shows the data captured by wired sensor for all the three sensor RF tags. It can be seen that the data matches with the wireless sensor RF tags as shown in Fig.5.7b, after applying harmonic rejection method.

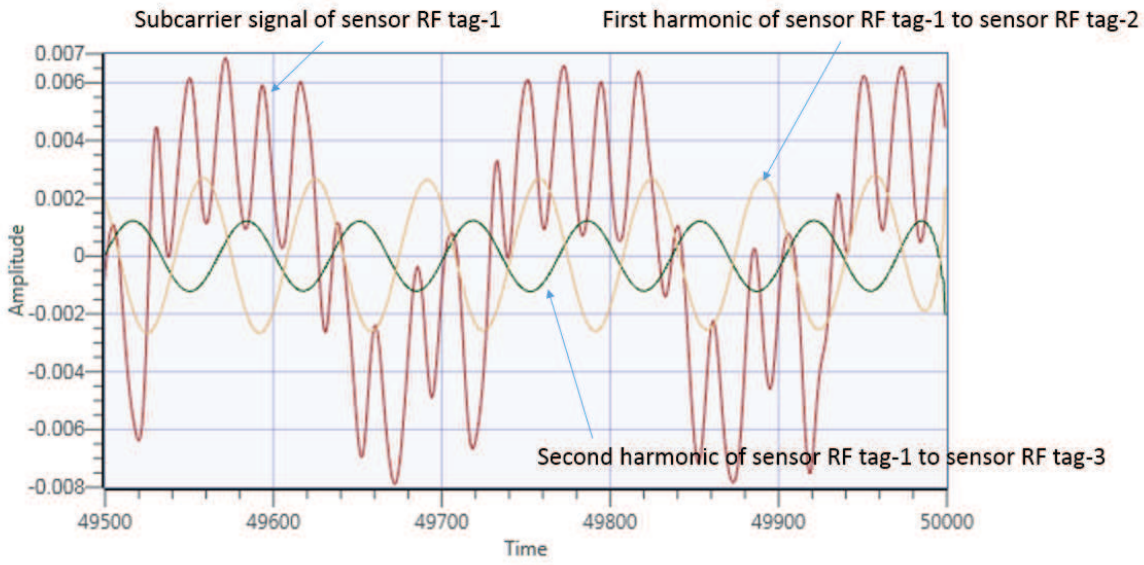

Figure 5.5: Harmonic interference from sensor RF tag-1 to sensor RF tag 2 and 3

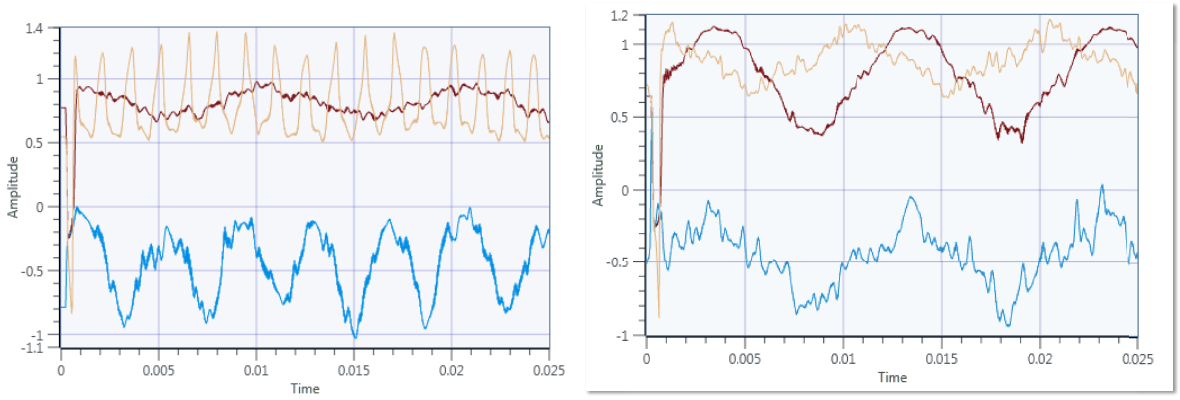

(a) The received signal from the sensor RF tags before applying harmonic rejection method

(b) Sensor RF tag original signal after harmonic rejection method.

Figure 5.6: Picture shows the signal received from the sensor RF tags before and after harmonic rejection method.

5.4 Summary

In this chapter, vibration testing setup is explained for three sensor RF tags and the results are presented. The experiment results are compared with the original signal captured by com-

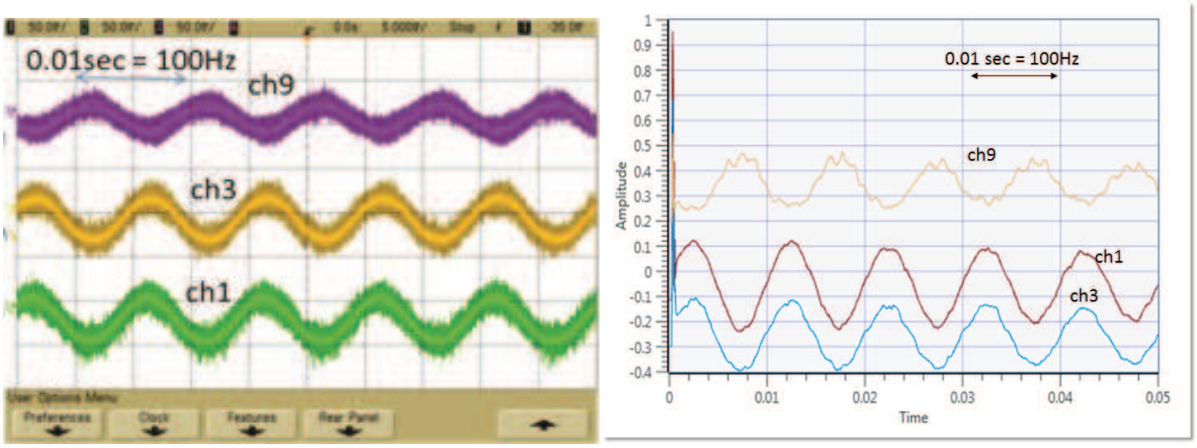

(a) (b)

Figure 5.7: Comparison of original signals with wired accelerometer sensors and wireless sensor RF tags

mercial wired vibration testing sensors. The results with the wired and wireless sensors are matched, showing that the harmonic rejection method works as expected.

Chapter 6

Conclusion

The objective of this research is to establish a multiple access method to enables concurrent data streaming from batteryless and wireless sensor RF tags.

As an answer to this objective, this research proposes a new multiple access method, referred to as Multiple Subcarrier Multiple Access (MSMA), tailored to ultra low functional batteryless and wireless sensors. MSMA can handle non-orthogonal subcarrier backscatters produced by multiple sensor RF tags and thus realize concurrent sensor data streaming. There are two challenges in this research. One is the harmonic rejection among subcarriers and the other is the optimization of subcarrier allocation.

The harmonics rejection is realized by carefully handling group delay and phase delay of the subcarrier envelope and the carrier signal to accurately produce replica of the harmonics by processing analytic signal generated from Hilbert transformation. The harmonic rejection method performance is evaluated with simulation and experiment to show that it can reconstruct the original sensor data wave shape with over 98 % accuracy in 0 dB CIR environment.

On the channel optimization problem, this research proposes a new evaluation criteria referred to as total contamination power to prioritize the channel allocation. The indecision case is to prioritize either a far RF tag with narrow band requirement or a near RF tag with wide band requirements. The allocation with total contamination power achieves almost the same

communication capacity to that of the brute force allocation, where all possible combinations are examined. Yet, the proposal only demand $O(n^2)$ computation time where the brute force demand $O(n!)$ examination.

Let us revisit the requirements toward this research explained in Chapter 1 and clarify how this research accommodates them.

- **The time synchronization should be below 120 μs.**
  MSMA realizes the multiple access concurrency by superposing sensor stream on the backscatter of powering continuous wave provided by a Reade/Writer. Since the inherent mutual interference among backscatters can be successfully rejected by the proposed harmonic rejection method asserted at the receiver of Reader/Writer, the remaining source of synchronization error is only the traveling time difference of radio wave, which are negligible in SHM arena. Therefore, the synchronization error of MSMA is virtually zero.

  The following two requirements are interrelated and thus revisited collectively.

- **The number of channels is up to 70 and at least 50.**

- **The target frequency bandwidth for one channel is up to 100 Hz.**
  MSMA supports both analog and digital modulation. Even in the case of digital modulation, where the required bandwidth is wider than that of the analog modulation, the subcarrier channels can be densely allocated. The dense allocation is enabled by the harmonics rejection and the optimal subcarrier allocation developed in this research. When we collect three axes acceleration data each of which consumes 100 Hz bandwidth, 10 kHz channel bandwidth should be sufficient even with digital modulation. MSMA can support, at least, 60 channels under Japan radio regulations where we can use up to 600 kHz single side band.

- **The proposed system should be implemented and verified with a vibration testing.** This research produces not only the theory of MSMA but also the prototype sensor RF tag, sensor RF tag firmware as well as the software defined Reader/Writer. The integrated software and hardware is applied to a vibration test with three sensors. It is proved the vibration testing using MSMA can achieve the equivalent accuracy and performance of wired vibration testing.

Bibliography

[1] http://www.mlit.go.jp/hakusyo/mlit/h25/. (visited June 4, 2017).

[2] http://www.mlit.go.jp/road/sisaku/yobohozen/yobohozen.html. (visited June 4, 2017).

[3] Sasago Tunnel Ceiling Collapse on the Chuo Expressway. https://www.mlit.go.jp/road/road_e/03key_challenges/1-2-1.pdf (visited June 4, 2017).

[4] Adee,S., Wireless Sensors That Live Forever, IEEE Spectrum, Jan. 29, (2010), pp.14-14.

[5] Analog Devices, MEMS wireless vibration sensing enables remote monitoring of industrial machine health, Analog device news release, June 4, (2013).

[6] Wang,Z., Bouwens,F., Vullers,R., Petre,F., Energy-autonomous wireless vibration sensor for condition-based maintenance of machinery, IEEE Sensors, (2011), pp.790-793.

[7] George,S.,E., Bocko,M., Nickerson,G.,W., Evaluation of a vibration powered wireless temperature sensor for health monitoring, IEEE Aerospace Conference, (2005), pp.3775-3781.

[8] Akhond,M.,R., Talevski,A., Cho,T.,H.,Prototype Design and Analysis ofWireless Vibration Sensor,International Conference on Broadband, Wireless Computing, Communication and Applications, (2010), pp.818- 823.

[9] Ministry of land, infrastructure, transport and tourism. http://www.mlit.go.jp/en/index.html. (visited June 4, 2017).

[10] A.B.Noel, A. Abdaoui, T.Elfouly, M.H.Ahmed, A.Badawy and M.Shehara. "Structural Health Monitoring using Wireless Sensor Networks: A Comprehensive Survey", IEEE Communications Survey, Issue 99, (2017).

[11] Xu, N., Rangwala, S., Chintalapudi, K. K., Ganesan, D., Broad, A., Govindan, R., & Estrin, D., "A wireless sensor network For structural monitoring," presented at the Proceedings of the 2nd international conference on Embedded networked sensor systems, Baltimore, MD, USA, (2004). pp.13-24

[12] Wang, P., Yan, Y., Tian, G. Y., Bouzid, O., & Ding, Z., "Investigation of wireless sensor networks for structural health monitoring". Journal of Sensors, Article ID 156329, (2012).

[13] E. Sazonov, V. Krishnamurthy, and R. Schilling. "Wireless intelligent sensor and actuator network-a scalable platform for time-synchronous applications of structural health monitoring," Structural Health Monitoring, vol. 9, no. 5, (2010). pp.465-476.

[14] ISO/IEC 18000-6, Information Technology - Radio frequency identification for item management- , Part 6 Parameters for air interface communications at 860 MHz to 960 MHz, (2010).

[15] Khasgiwale,R., Adyanthaya, R., Engels, Daniel., "Extracting information from tag collisions" IEEE RFID, 2009 (2009), pp.131-138.

[16] Kineo-Battery free orientation sensor tag, http://www.farsens.com/en/product/3/kineo1-battery-free-orientation-sensor-tag. (visited May 14, 2017).

[17] GS1 EPCglobal, "The GS1 EPCglobal Architecture Framework" GS1 Version 1.7 dated 18 April 2015, http://www.gs1.org/sites/default/files/docs/architecture/EPC architecture 1 7-framework-May-2015.pdf.

[18] Vahedi,E., Ward,R.,K., Blacke,I.,F., “Performance Analysis of RFID Protocols: CDMA Versus the Standard EPC Gen-2” IEEE Trans. Automation Science and Engineering,vol.11, no.4, Oct. (2014), pp.1250-1261.

[19] Paggi, C., C. Occhiuzzi, and G. Marrocco. “Sub-millimeter displacement sensing by passive UHF RFID antennas.” IEEE Transactions on Antennas and Propagation 62.2 (2014), pp.905-912.

[20] Alamin, M., Tian, G. Y., Andrews, A., & Jackson, “Corrosion detection using low-frequency RFID technology.” Insight-Non-Destructive Testing and Condition Monitoring 54.2 (2012), pp.72-75.

[21] Ikemoto, Y., Suzuki, S., Okamoto, H., Murakami, H., Asama, H., Morishita, S., & Itoh, H. “Force sensor system for structural health monitoring using passive RFID tags.” Sensor Review 29.2 (2009), pp.127-136.

[22] Occhiuzzi, C., C. Paggi, and G. Marrocco. “Passive RFID strain-sensor based on meander-line antennas.” IEEE Transactions on Antennas and Propagation 59.12 (2011), pp.4836-4840.

[23] Stockman, Harry. “Communication by means of reflected power.” Proceedings of the IRE 36.10 (1948), pp.1196-1204.

[24] Talla,V., Smith, J.,R.,“Hybrid analog-digital backscatter: A new approach for battery-free sensing”, IEEE International Conference on RFID,(2013), pp.74- 81.

[25] Teramoto,S., Ohtsuki,T., “Multiple-Subcarrier Optical Communication Systems With Subcarrier Signal-Point Sequence”, IEEE Trans. Communications, vol.53, no.10, (2005), pp.1738-1743.

[26] Cnaan-On, I., Thomas, S. J., Reynolds, M. S., & Krolik, J. L., "Multichannel radar backscatter communication and localization.", Acoustics, Speech and Signal Processing (ICASSP), 2014 IEEE International Conference on. IEEE, (2014), pp.76-80.

[27] Cnaan-On, I., Thomas, S. J., Krolik, J. L., & Reynolds, M. S., "Multichannel Backscatter Communication and Ranging for Distributed Sensing With an FMCW Radar." IEEE Transactions on Microwave Theory and Techniques 63.7 (2015), pp.2375-2383.

[28] Shen,D., Woo,G., Reed,D., Lippman,A., Wang,J., "Separation of multiple passive RFID signals using Software Defined Radio" IEEE RFID, 2009 (2009), pp.139-146.

[29] Wang, J., Hassanieh, H., Katabi, D., & Indyk, P. "Efficient and reliable low-power backscatter networks". In Proceedings of the ACM SIGCOMM 2012 conference on Applications, technologies, architectures, and protocols for computer communication, (2012), pp. 61-72.

[30] Angerer, C., Langwieser, R., & Rupp, M. (2010). "RFID reader receivers for physical layer collision recovery". IEEE Transactions on Communications, 58(12), (2010), pp.3526-3537.

[31] Hu, P., Zhang, P. and Ganesan, D., "Laissez-faire: Fully asymmetric backscatter communication". In ACM SIGCOMM Computer Communication Review Vol. 45, No. 4, (2015), pp. 255-267. pp.255-267.

[32] Zhang, Y., Amin, M. and Ahmad, F., "Time-frequency analysis for the localization of multiple moving targets using dual-frequency radars". IEEE Signal Processing Letters, 15, (2008), pp.777-780.

[33] Weldon, J. A., Narayanaswami, R. S., Rudell, J. C., Lin, L., Otsuka, M., Dedieu, S., & Gray, P. R., "A 1.75-GHz highly integrated narrow-band CMOS transmitter

with harmonic-rejection mixers". IEEE Journal of Solid-State Circuits, 36(12), (2001), pp.2003-2015.

[34] Li, C., Li, M., Verhelst, M., Bourdoux, A., Van der Perre, L., & Pollin, S. "On the general mathematical framework, calibration/compensation method, and applications of non-ideal software defined harmonics rejection transceivers." IEEE Transactions on Circuits and Systems I: Regular Papers 62.1 (2015), pp.292-301.

[35] Saldanha,N, Malocha,D.,C., "Pseudo-orthogonal frequency coded wireless SAW RFID temperature sensor tags" IEEE Trans. Ultrasonics, Ferroelectrics, and Frequency Control, vol.59, no.8, (2012), pp.1750-1758.

[36] Gungor, V. C., & Hancke, G. P., "Industrial wireless sensor networks: Challenges, design principles, and technical approaches". IEEE Transactions on industrial electronics, (2009), pp.4258-4265.

[37] Hou, Z., Wu, D.,& Cai, Y., "Subcarrier and power allocation in uplink multi-cell OFDMA systems based on game theory". In Communication Technology (ICCT), 2010 12th IEEE International Conference, (2010), pp. 1113-1116.

[38] Yan, T., Yayan, M., & Baoyun, W., "Energy-efficient power control and subcarrier allocation in OFDMA systems based on game theory". In High Mobility Wireless Communications (HMWC), 2014 International Workshop, (2014), pp. 130-134.

[39] Zheng, K., Hu, F., Wang, W., Xiang, W., & Dohler, M., "Radio resource allocation in LTE-advanced cellular networks with M2M communications". IEEE communications Magazine, (2012), pp.184-192. .

[40] Jain, R., Chiu, D. M., & Hawe, W. R., "A quantitative measure of fairness and discrimination for resource allocation in shared computer system", (Vol. 38). Hudson, MA: Eastern Research Laboratory, Digital Equipment Corporation, (1984).

[41] Sample, A. P., Yeager, D. J., Powledge, P. S., Mamishev, A. V., & Smith, J. R., "Design of an RFID-based battery-free programmable sensing platform." IEEE Transactions on Instrumentation and Measurement 57.11 (2008), pp.2608-2615.

[42] Analog Devices ADXL362 Accelerometer, http://www.analog.com/en/mems-sensors/mems-accelerometers/adxl362/products/product.html. (visited June 4, 2017).

[43] Shannon,C.,E., "A Mathematical Theory of Communication", Bell System Technical Journal, vol.27, (1948), pp.379-423.

[44] http://tractool.seamcat.org/wiki/Manual/PropagationModels/ ExtendedHata SRD. (visited May 29, 2017).